Available online at www.sciencedirect.com

ScienceDirect

Geochimica et Cosmochimica Acta 164 (2015) 333–351

Geochimica et Cosmochimica Acta

www.elsevier.com/locate/gca

Magnesium isotopic compositions of the Mesoproterozoic dolostones: Implications for Mg isotopic systematics of marine carbonates

Kang-Jun Huang [a], Bing Shen [a,*], Xian-Guo Lang [a], Wen-Bo Tang [b], Yang Peng [a], Shan Ke [c], Alan J. Kaufman [d], Hao-Ran Ma [a], Fang-Bing Li [a]

[a] *Key Laboratory of Orogenic Belts and Crustal Evolution, MOE & School of Earth and Space Sciences, Peking University, Beijing 100871, PR China*

[b] *School of Mathematical & Statistical Sciences, Arizona State University, Tempe, AZ 85287, USA*

[c] *State Key Laboratory of Geological Processes and Mineral Resources, China University of Geosciences, Beijing 100083, PR China*

[d] *Department of Geology, University of Maryland, College Park, MD 20742-2465, USA*

Received 30 July 2014; accepted in revised form 4 May 2015; Available online 16 May 2015

Abstract

Available Mg isotope data indicate that dolostones of different ages have overlapping range of Mg isotopic composition (δ^{26}Mg) and there is no systematic difference among different types of dolomites. To further explore the Mg isotopic systematics of dolomite formation, we measured Mg isotopic compositions of Mesoproterozoic dolostones from the Wumishan Formation in North China Block, because dolomite formation in Mesoproterozoic might have been fundamentally different from the younger counterparts. Based on petrographic observations, three texturally-different dolomite phases (dolomicrite, subhedral dolomite and anhedral dolomite) are recognized in the Wumishan dolostones. Nevertheless, these three types of dolomites have similar δ^{26}Mg values, ranging from −1.35‰ to −1.72‰, which are indistinguishable from Neoproterozoic and Phanerozoic dolostones. To explain δ^{26}Mg values of dolostones, we simulate the Mg isotopic system during dolomite formation by applying the one-dimensional Diffusion–Advection–Reaction (1D-DAR) model, assuming that the contemporaneous seawater is the Mg source of dolostone. The 1D-DAR modeling results indicate that the degree of dolomitization is controlled by sedimentation rate, seawater Mg concentration, temperature, and reaction rate of dolomite formation, whereas Mg isotopic composition of dolostone is not only dependent on these factors, but also affected by δ^{26}Mg of seawater and isotope fractionation during dolomite formation. Moreover, the 1D-DAR model predicts that dolomite formation within sediments has limited range of variation in δ^{26}Mg with respect to limestones. Furthermore, the modeling results demonstrate that dolostone is always isotopically heavier than Ca-carbonate precipitated from seawater, explaining the systematic isotopic difference between dolostones and limestones. Finally, we can infer from the 1D-DAR model that early-formed dolostone at shallower depth of sediments is always isotopically lighter than that formed in deeper sediments, suggesting the potential application of Mg isotope as a proxy for constraining dolostone formation.

1. INTRODUCTION

Presence of abundant massive dolostone in the rock records is in sharp contrast to the scarcity of dolomite formation in modern environments, collectively termed the

* Corresponding author.
E-mail address: bingshen@pku.edu.cn (B. Shen).

http://dx.doi.org/10.1016/j.gca.2015.05.002
0016-7037/

'dolomite problem' (Holland and Zimmermann, 2000), which is exemplified by the following observations. Firstly, modern dolomite formation is restricted in a few localities that are normally characterized by special hydrological and/or geochemical conditions (Last, 1990; Vasconcelos and McKenzie, 1997). In contrast, ancient dolostones have a wide range of paleogeographic distributions, and many of them might have deposited under normal marine conditions (Mackenzie and Morse, 1992; Holland and Zimmermann, 2000; Hood et al., 2011). Secondly, modern dolomite is typically represented by discrete thin-layers within calcareous sediments (Vasconcelos and McKenzie, 1997; Warthmann et al., 2000). However, ancient dolostone sequence could be hundreds to thousands of meters in thickness (Mackenzie and Morse, 1992; McKenzie and Vasconcelos, 2009). Thirdly, most modern dolomite is poorly ordered, whereas nearly all ancient dolostones are stoichiometric (Warren, 2000). Such differences are also echoed by the failure of laboratory precipitation of dolomite at room temperature, suggesting that inorganic dolomite formation in ambient marine conditions is not thermodynamically favored (Land, 1992). Since two decades ago, there is growing realization that modern dolomite precipitation could be significantly enhanced by microbial activities or the product of microbe-mediated reactions (e.g., H_2S) (Vasconcelos et al., 1995; Warthmann et al., 2000; Zhang et al., 2012a). Furthermore, dolomite precipitation could be stimulated by the presence of organic molecules (Roberts et al., 2013). However, it is still unclear whether organogenic dolomitization could be an important component for ancient massive dolostone formation. Therefore, the origin of ancient dolostone is still a big challenge in spite of rapid progresses in the study of modern dolomite formation.

Conventional stable and radiogenic isotope systems, trace element geochemistry as well as petrographic approaches (e.g., Tucker, 1983; Aulstead et al., 1988; Last, 1990; Vasconcelos et al., 1995; Budd, 1997; Warren, 2000; Machel, 2004; Zhang et al., 2012b; Mathieu et al., 2013) are generally applied to ancient dolostone studies. However, none of these traditional approaches can provide unambiguous solution to the origin of ancient dolostone. With the advent of high resolution multiple-collector inductively coupled plasma-source mass spectrometry (MC-ICPMS) in the last decade (Plummer et al., 1998), high precision Mg stable isotope measurement provides a promising approach to study the origin of ancient dolostones in the geological history (Galy et al., 2002; Young and Galy, 2004; Higgins and Schrag, 2010). The main reasons are (1) Mg is a key element in dolomite, and the potential Mg sources for dolomite formation, including terrestrial silicates, carbonate sediments and seawater, have distinct Mg isotopic compositions (Ref. Li et al., 2012; Wang et al., 2012a); and (2) Mg isotopes fractionate significantly during dolomite (Higgins and Schrag, 2010; Rustad et al., 2010; Schauble, 2011; Mavromatis et al., 2014; Geske et al., 2015b) and other carbonate minerals precipitation (Immenhauser et al., 2010; Li et al., 2012; Pearce et al., 2012; Saulnier et al., 2012; Wang et al., 2012b) with preferential uptake of light Mg isotopes into minerals. As such, Mg isotopes may provide valuable insight into the origin of dolomite (Higgins and Schrag, 2010; Fantle and Higgins, 2014; Geske et al., 2015a).

Current available Mg isotope data indicate that there is no secular trend in the Mg isotopic composition of ancient dolostone, nor there is any systematic isotopic difference among different types of dolomites (Azmy et al., 2013; Geske et al., 2015a), suggesting that using Mg isotopes to constrain the origin of ancient dolostone might not be straightforward. Except for a few studies of Neoproterozoic dolostones (e.g., Pokrovsky et al., 2011; Kasemann et al., 2014; Liu et al., 2014), previous studies are mainly focused on Phanerozoic and modern samples (e.g., Higgins and Schrag, 2010; Fantle and Higgins, 2014; Mavromatis et al., 2014; Geske et al., 2015a). So far, little is known about the Mg isotopic compositions of older dolostones, for example, Mesoproterozoic dolostones.

To further understand the Mg isotopic system during ancient dolostones formation, we focus on Mesoproterozoic dolostones in this study. The reason for selection of Mesoproterozoic dolostones is because current understanding of Mesoproterozoic carbonate depositional system might be fundamentally different from that of younger ages (Grotzinger and Knoll, 1995; Kah and Riding, 2007). There is a consensus that the dolomite abundance was high during much of the Proterozoic (Mackenzie and Morse, 1992; Holland and Zimmermann, 2000; Hood et al., 2011), resulting in a conceivable interpretation that Precambrian seawater permitted direct dolomite precipitation from seawater and/or extensive dolomitization in carbonate rocks (Tucker, 1982). Therefore, we speculate that the Mg isotopic system of Mesoproterozoic dolostone might be different from their younger counterparts. As one of the main sinks of seawater Mg (Mackenzie and Morse, 1992), dolomite deposition plays an important role in regulating seawater δ^{26}Mg over geological time scales (Fantle and Higgins, 2014; Kasemann et al., 2014; Pogge von Strandmann et al., 2014). Hence, in theory, Mesoproterozoic seawater might have heavier δ^{26}Mg since light Mg isotopes are preferentially scavenged from seawater during massive dolostone formation (Tipper et al., 2006; Higgins and Schrag, 2015). Consequently, Mesoproterozoic dolomites would have relatively heavier δ^{26}Mg values.

To test whether Mg isotopic systems of Mesoproterozoic and younger dolostones are significantly different, in this study we measured Mg isotopic compositions of dolostone samples collected from the Mesoproterozoic Wumishan Formation in North China Block. The reason to choose these samples is because the Wumishan dolostone is the representative Mesoproterozoic carbonate deposition in North China, and is composed of laminated and thrombolytic/stromatolitic dolostones, which are the typical lithologies of Mesoproterozoic carbonates. Our data show that Mg isotopic compositions of the Mesoproterozoic Wumishan dolostones are indistinguishable from younger dolostones. To further interpret the invariant Mg isotopic data, we develop the one-dimensional Diffusion–Advection–Reaction (1D-DAR) model to quantify the Mg isotopic system of dolomite formation.

2. GEOLOGICAL BACKGROUND AND SAMPLE DESCRIPTION

2.1. Geological background

Dolostone samples were collected from the Mesoproterozoic Wumishan Formation in the Jixian area, North China (Fig. 1A). The Palaeoproterozoic–Mesoprot erozoic successions in the Jixian area are represented by, in ascending order, the Changcheng, Jixian, and Qingbaikou groups (Ren et al., 2007; Lu et al., 2008). The Jixian Group consists of four lithological units, in stratigraphic order, the Yangzhuang, Wumishan, Hongshuizhuang, and Tieling formations. The Wumishan Formation is about 3300 m thick in this region, and conformably overlies the sandy dolostone of the Yangzhuang Formation and is underlain by the black shale of the Hongshuizhuang Formation (Mei et al., 2010). The age of the Wumishan Formation is loosely constrained between ca. 1.6 and 1.3 billion years ago (Ga), based on the SHRIMP zircon U–Pb dating from the underlain Gaoyuzhuang Formation (ca.1.53 ~ ca.1.60 Ga) and the overlying Xiamaling Formation (ca.1.30 ~ ca.1.40 Ga) (Gao et al., 2010; Tang et al., 2013).

The dolostone samples were collected from the middle part of the Wumishan Formation in the Mopanyu section, northern Jixian County. In this section, the Wumishan Formation is composed of cyclic meter-scale shoaling-upward sequence, consisting of calcareous shale (CS)-massive microbial dolostone/thrombolites (MMD)-microbial laminated dolostone (LD) (Mei et al., 2001) (Fig. 1B). The basal CS unit is interpreted as the deposition in the lower sub-tidal environment. The transition from the CS unit to the MMD unit is gradual, as evident by the gradual decrease in siliciclastic contents. The MMD unit may be deposited in the upper sub-tidal environment, while the overlying LD unit might have deposited in the upper sub-tidal to inter-tidal conditions (Mei et al., 2010; Tang et al., 2013). Chert bands/nodules, varying from 2 mm to 10 cm in thickness/diameter, are abundantly distributing in the LD unit.

2.2. Sample descriptions

Four dolostone specimens were collected from the LD unit of the Wumishan Formation in the Mopanyu section (Fig. 1B). The laminae of the LD unit are defined by the alternations of three types of dolomite with different textures. The contact between the adjacent laminae is clear and sharp. The type 1 dolomite (D1) is composed of dolomicrite and microcrystalline dolomite (crystal size <50 μm), characterized by euhedral crystals with planar crystal edges (Fig. 2A). This suggests an early formation within shallow depth of sediments, probably representing syn-sedimentary in origin. The type 2 dolomite (D2) is composed of sub-euhedral fine- to medium-grained dolomite with sub-planar crystals. The D2 dolomite varies from 50 μm to 200 μm in size and has a cloudy core and clear rim (Fig. 2B and C), suggesting the replacement in origin (Sibley and Gregg, 1987; Warren, 2000). The type 3 dolomite (D3) has anhedral coarse-grained crystals, which is typical for late dolomite formation at relatively high

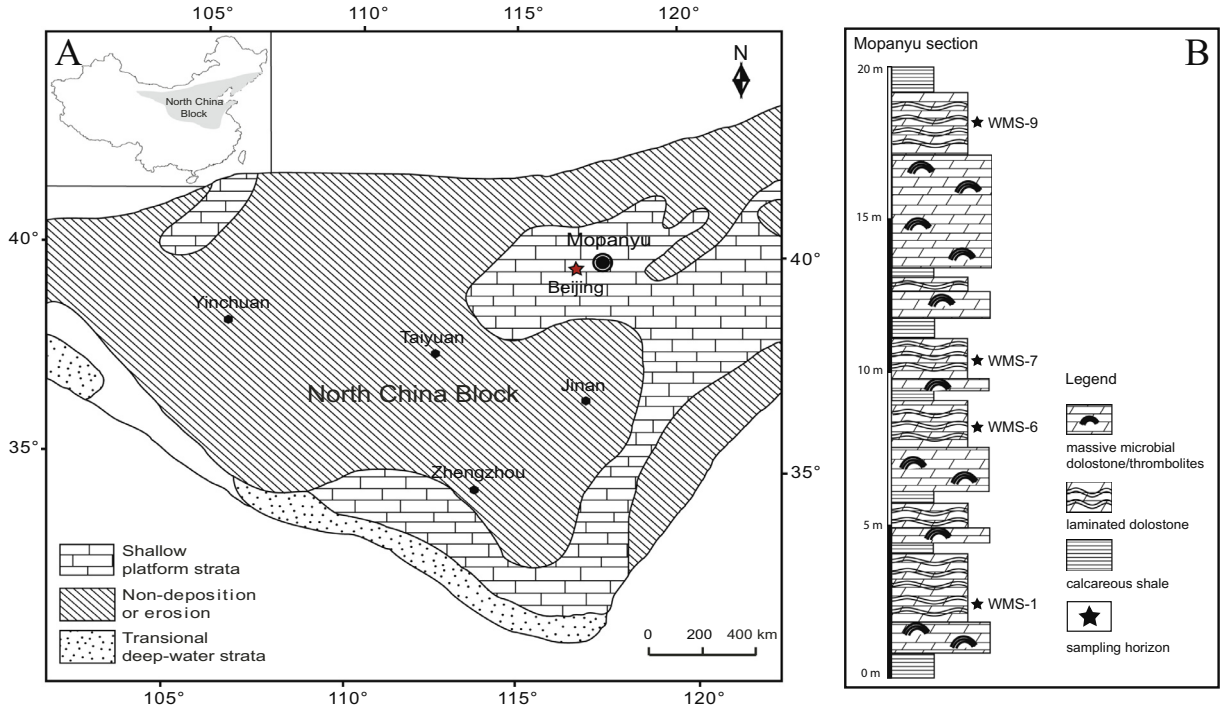

Fig. 1. (A) Simplified paleogeographic map of the North China Block (modified from Chu et al., 2007) showing the sampling locality in the Mopanyu section (concentric circle); inset showing the current geographic location of North China Block. (B) The measured stratigraphic column of the Wumishan Formation in the Mopanyu section in the Jixian County. Sampling horizons are shown by black stars.

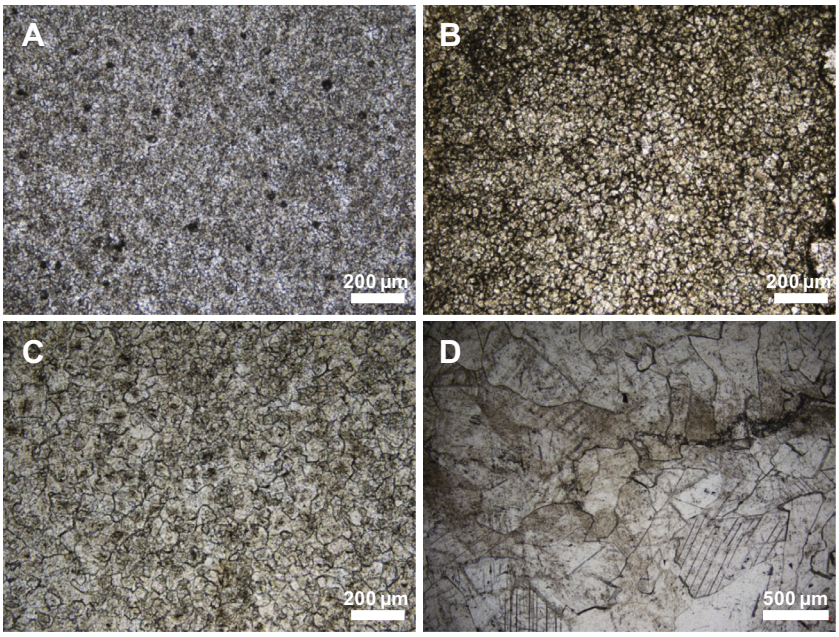

Fig. 2. Photomicrographs of three dolomite types investigated in the Mesoproterozoic Wumishan Formation under plane polarized light. (A) Type 1 dolomite (D1): euhedral dolomicrite (sample WMS-1); (B) Type 2 dolomite (D2): subhedral fine- to medium-grained dolomite (sample WMS-6); (C) Type 2 dolomite (D2): nonplanar coarse-grained dolomite (sample WMS-7); (D) Type 3 dolomite (D3): anhedral coarse-grained dolomite (sample WMS-9).

temperature (Sibley and Gregg, 1987). Some D3 dolomite crystals are non-planar to xenotopic with crystal sizes larger than 500 μm (Fig. 2D). There is no general trend for the distribution of the three types of dolomites in the Wumishan dolostones. Overall, samples WMS-1 and WMS-9 contain all three types of dolomites, while samples WMS-6 and WMS-7 are dominated by D2 and D3 dolomites, respectively (Table 1).

3. METHODOLOGY

3.1. Sample preparation

Mirrored thin and thick sections were prepared for micro-mill sampling. Under the guidance of thin section observation, sample powders were micro-drilled from the corresponding localities in the polished thick section. In order to compare the Mg isotopic compositions among different types of dolomites, multiple samples were collected from the same specimen. About 1 mg of dolomite powder was collected in each sample. Five D1 dolomite, eleven D2 dolomite, and ten D3 dolomite samples were collected from four specimens (Table 1). Powder samples were separated into two aliquots for Mg and C/O isotopes analyses. One aliquot of sample powder was placed into 15 ml centrifuge tubes and dissolved in 0.5 N acetic acid. Centrifuge tubes were then placed in an ultrasonic bath for 30 min, and were centrifuged at 3000 rpm for 10 min. The supernatant was collected and separated into two parts. One was used for major elemental (Mg and Ca) analyses on a Leeman Prodigy inductively-coupled plasma optical emission spectrometry (ICP-OES) at China University of Geosciences, Beijing, and the other was ready for Mg isotopic analysis.

3.2. Carbon and oxygen isotopes

Sample powders were reacted for 10 min at 90 °C with anhydrous H_3PO4 with a Multiprep inlet system on-line with a dual inlet Isoprime gas source mass spectrometer in the Stable Isotope Facility of the University of Maryland Geochemical Laboratories (cf., Kaufman et al., 2007). All isotope ratios are expressed in the standard δ notation as per mil (‰) deviation from the Vienna-Pee Dee Formation belemnite (V-PDB) international standard. Uncertainties determined by multiple analyses of a laboratory standard carbonate (calibrated to NBS-19) during each run of samples were 0.1‰ for $\delta^{13}C$ and 0.2‰ for $\delta^{18}O$.

3.3. Magnesium isotopes

Magnesium was purified by cation exchange chromatography at Peking University. In this procedure, two columns were used to purify Mg from other matrix metals (Shen et al., 2009, 2013). Column #1, designated to separate Mg from Ca, was loaded with 1.8 ml of Bio-Rad AG50W-X12 resin (200–400 mesh). Sample solution containing 25 ~ 30 μg of Mg was eluted by 10 N HCl. Mg fraction was collected in 4 ml of 10 N HCl, while Ca was retained in the resin. Column #2 was loaded with 0.5 ml of Bio-Rad AG50W-X12 resin (200–400 mesh), and used to separate Mg from all other matrix. This step involves the sequential elution of 0.8 ml of 1 N HCl, 3 ml of 1 N HNO_3 + 0.5 N HF, and 1 ml of 1 N HNO_3 to elute Cr,

Table 1
Measured Mg isotopic compositions, Mg/Ca ratios, $\delta^{13}C$ and $\delta^{18}O$ values for dolostone samples from the Mesoproterozoic Wumishan Formation in North China Block.

Sample no.	Description	Type	Mg/Ca (mol/mol)	$\delta^{13}C$ (‰)	$\delta^{18}O$ (‰)	$\delta^{25}Mg \pm 2SD$ (‰)	$\delta^{26}Mg \pm 2SD$ (‰)
WMS 1-1	Subhedral–anhedral dolomite, 30 ~ 80 μm crystal size	D2	0.98	−0.94	−5.77	−0.77 ± 0.03	−1.48 ± 0.06
WMS 1-2	Euhedral–subhedral dolomite, 5 ~ 20 μm crystal size	D1	0.99	−1.30	−5.16	−0.89 ± 0.03	−1.72 ± 0.04
WMS 1-3	Subhedral–anhedral dolomite, 100 ~ 300 μm crystal size	D3	0.99	−1.02	−6.15	−0.89 ± 0.02	−1.70 ± 0.02
WMS 1-4	Subhedral–anhedral dolomite, 30 ~ 120 μm crystal size	D3	0.98	−0.81	−7.60	−0.81 ± 0.02	−1.57 ± 0.06
WMS 1-5	Anhedral dolomite, 100 ~ 300 μm crystal size	D3	1.02	−0.90	−6.87	−0.86 ± 0.04	−1.67 ± 0.06
WMS 1-5R	Replicate					−0.86 ± 0.03	−1.69 ± 0.05
WMS 6-1	Euhedral–subhedral dolomite, 10 ~ 50 μm crystal size	D2	0.96	−0.86	−4.88	−0.76 ± 0.03	−1.46 ± 0.04
WMS 6-2	Euhedral–subhedral dolomite, 50 ~ 100 μm crystal size	D2	0.97	−0.77	−4.95	−0.77 ± 0.04	−1.50 ± 0.03
WMS 6-3	Euhedral–subhedral dolomite, 30 ~ 80 μm crystal size	D2	0.96	−0.75	−4.72	−0.74 ± 0.05	−1.49 ± 0.07
WMS 6-4	Euhedral–subhedral dolomite, 50 ~ 150 μm crystal size	D2	0.97	−0.75	−4.75	−0.76 ± 0.06	−1.46 ± 0.02
WMS 6-5	Equant, euhedral–subhedral dolomite, 20 ~ 40 μm crystal size	D2	0.96	−0.86	−5.13	−0.75 ± 0.01	−1.43 ± 0.05
WMS 6-6	Euhedral–subhedral dolomite, 30 ~ 80 μm crystal size	D2	0.98	−0.94	−5.13	−0.80 ± 0.04	−1.52 ± 0.04
WMS 6-7	Equant, euhedral–subhedral dolomite, 30 ~ 50 μm crystal size	D2	1.01	−0.87	−4.83	−0.77 ± 0.05	−1.49 ± 0.07
WMS 6-8	Euhedral–subhedral dolomite, 50 ~ 100 μm crystal size	D2	0.97	−0.75	−4.88	−0.75 ± 0.07	−1.49 ± 0.03
WMS 6-9	Equant, euhedral–subhedral dolomite, 20 ~ 30 μm crystal size	D1	1.01	−1.25	−4.92	−0.84 ± 0.01	−1.63 ± 0.02
WMS 7-1	Subhedral–anhedral dolomite, 100 ~ 300 μm crystal size	D3	1.02	−0.89	−6.19	−0.73 ± 0.03	−1.43 ± 0.02
WMS 7-2	Subhedral–anhedral dolomite, 50 ~ 200 μm crystal size	D3	0.98	−0.90	−6.42	−0.76 ± 0.08	−1.46 ± 0.03
WMS 7-3	Subhedral–anhedral dolomite, 200 ~ 400 μm crystal size	D3	0.98	−0.75	−5.90	−0.72 ± 0.06	−1.37 ± 0.03
WMS 7-4	Subhedral–anhedral dolomite, 200 ~ 500 μm crystal size	D3	0.99	−0.86	−6.32	−0.76 ± 0.04	−1.48 ± 0.04
WMS 9-1	Euhedral–subhedral dolomite, <10 μm crystal size	D1	0.98	−1.26	−5.97	−0.72 ± 0.06	−1.41 ± 0.03
WMS 9-2	Euhedral–subhedral dolomite, 100 ~ 200 μm crystal size	D3	0.98	−1.09	−6.32	−0.73 ± 0.03	−1.40 ± 0.05
WMS 9-3	Subhedral–anhedral dolomite, crystal size >300 μm	D3		−1.07	−7.77	−0.69 ± 0.05	−1.35 ± 0.02
WMS 9-4	Euhedral–subhedral dolomite, crystal size 40 ~ 80 μ	D2	0.98	−1.11	−6.17	−0.84 ± 0.02	−1.61 ± 0.01
WMS 9-5	Euhedral–subhedral dolomite, crystal size <10 μm	D1	0.99	−1.22	−6.50	−0.72 ± 0.02	−1.42 ± 0.04
WMS 9-6	Subhedral–anhedral dolomite, crystal size 120 ~ 200 μm	D3	0.98	−1.29	−6.76	−0.82 ± 0.07	−1.60 ± 0.05
WMS 9-7	Euhedral–subhedral dolomite crystal size 80 ~ 120 μm	D2	0.98	−1.20	−5.99	−0.73 ± 0.03	−1.39 ± 0.07
WMS 9-8	Euhedral–subhedral dolomite, crystal size 80 ~ 120 μm	D2	1.01	−1.29	−5.94	−0.82 ± 0.04	−1.58 ± 0.03

2SD = 2 times the standard deviation of the population of n ($n > 3$) repeat measurements of the standards during an analytical session.
'Replicate' refers to repeat column chemistry and instrumental measurement of different aliquots of the same stock solution.
D1, D2, D3 refer to different dolomite phases in massive dolostone on the basis of petrographic observations in thin sections.
The precisions determined by multiple analyses of the laboratory standard carbonate are 0.1‰ for $\delta^{13}C$ and 0.2‰ for $\delta^{18}O$.

Al, Fe, Na, V, and K, respectively. Mg fraction was then collected with 5 ml of 2 N HNO_3. To ensure a clean Mg fraction, each sample was passed through column #1 twice, followed by three passes of column #2. The recovery of Mg after the whole procedure of column chemistry was better than 99%. The total blank for the complete analysis was 10 ng Mg, which is insignificant compared to the mass of sample used. In addition to two USGS standards (BHVO-2 and BCR-2), synthetic solutions made by mixing $MgCl_2$ and $CaCl_2$ with molar ratio of 1:10, and pure $MgCl_2$ solution were processed with samples for the whole procedure of column chemistry as yet no carbonate reference standard for Mg isotopes exists.

Magnesium isotope ratios were measured by a Thermo Scientific Neptune Plus high-resolution MC-ICPMS at the Isotope Laboratory of China University of Geosciences, Beijing. Samples were measured using the standard-sample-standard bracketing method to correct for the instrumental mass bias and drift. An in-house standard solution (Mg-FZT) was used as the standard. Solutions containing 400 ppb Mg were introduced into the plasma (~50 μL/min) via a standard H-skimmer cone and an ESI PFA MicroFlow nebulizer with a quartz Scott-type spray chamber. Analyses were performed in low-resolution mode, simultaneously measuring ^{26}Mg, ^{25}Mg, and ^{24}Mg isotopes. A 400 ppb solution typically yields a ^{24}Mg signal of ~6 V, while the blank was typically $<10^{-4}$ V of ^{24}Mg, negligible relative to the sample signals. The measured Mg isotope ratios are reported in the delta notation as per mil (‰) deviation relative to the DSM3 standard (Galy et al., 2003): $\delta^x Mg = \left[\frac{\left(^xMg/^{24}Mg\right)_{sample}}{\left(^xMg/^{24}Mg\right)_{DSM3}}\right] \times 10^3$, where x refers to 25 or 26.

All samples were analyzed three times within an analytical session. The internal precision determined on the basis of ⩾3 repeated runs of the same sample solution during a single analytical session was better than ±0.10‰ (2SD). The external precision was determined by measurements of synthetic solution (GSB-Mg), USGS basalt standards (BHVO-2 and BCR-2). Multiple analyses of synthetic solution (GSB-Mg) yield average $\delta^{26}Mg$ value of −2.06‰ (Table 1), which is within the preferred error bound (−2.05 ± 0.05‰ (2σ). The USGS basalt standards, BCR-2 and BHVO-2 have average $\delta^{26}Mg$ values of −0.11 ± 0.05‰ (2σ) and −0.34 ± 0.07‰ (2σ), respectively, consistent with the published values (Ref. Huang et al., 2011; Teng et al., 2015). Two synthetic solutions, $MgCl_2$ and $CaCl_2$ with molar ratio of 1:10 and the pure $MgCl_2$ solution, have $\delta^{26}Mg$ values of −3.73 ± 0.10‰ and −3.93 ± 0.10‰, respectively (Table 1).

4. RESULT

Magnesium, carbon and oxygen isotopic compositions along with the Mg/Ca molar ratios of the Wumishan dolomite samples are listed in Table 1.

Three types of dolomite (D1, D2, and D3) recognized by the petrographic observations have similar Mg/Ca molar ratio of 1 (0.96–1.02) (Table 1), suggesting nearly stoichiometric dolomite compositions.

The Mg isotope data are presented in a three-isotope plot (Fig. 3). All the samples and standards analyzed in this study fall in a single isotopic mass-dependent fractionation line with a slope of 0.52. All types of dolomites have overlapping ranges of $\delta^{26}Mg$ values (Fig. 4). $\delta^{26}Mg$ values of the euhedral dolomicrites (D1), subhedral fine- to medium-grained dolomites (D2), and anhedral coarse-grained dolomites (D3) vary from −1.41‰ to −1.72‰, −1.39‰ to −1.61‰, and −1.35‰ to −1.70‰, respectively. Particularly, different types of dolomites in the same specimen have limited variations in $\delta^{26}Mg$ values. The maximum variation in $\delta^{26}Mg$ values observed in the same specimen is ~0.24‰ for sample WMS-1 (Table 1).

The $\delta^{13}C$ data of all types of dolomites span a small range from −0.75‰ to −1.30‰ (Table 1). There is no obvious difference in $\delta^{13}C$ among these three types of dolomites. Similarly, three types of dolomites have small variations in $\delta^{18}O$, varying from −4.72‰ to −7.60‰ (Table 1). Overall, $\delta^{18}O$ values for the D3 dolomites are systematically lighter than the D1 and D2 dolomites, which have similar ranges of $\delta^{18}O$ values. Moreover, $\delta^{18}O$ values show little covariation with $\delta^{13}C$ and $\delta^{26}Mg$ values for three types of dolomites (Fig. 5).

5. DISCUSSION

5.1. Evaluation of diagenetic alteration

Various studies have indicated that Mg isotopic composition of dolomite might have been preserved during diagenesis, dedolomitization and low grade metamorphism (Jacobson et al., 2010; Geske et al., 2012; Azmy et al., 2013), it is unclear whether Mg isotopes would be altered during some specific diagenetic processes, such as recrystallization or neomorphism. It is proposed that dolomite texture can be used as a diagnostic proxy to constrain the origin of dolomites (Sibley and Gregg, 1987). However, it is also conceivable that some textures could also be resulted from recrystallization or neomorphism. Thus, it is still

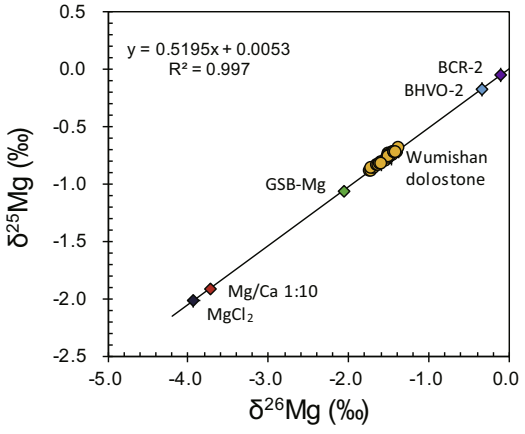

Fig. 3. Three isotope plot illustrating Mg isotopic composition for the Wumishan dolostones, USGS standards (BCR-2, BHVO-2), and synthetic solutions (GSB-Mg, $MgCl_2$, Mg/Ca 1:10). Solid line shows the regression line of all data.

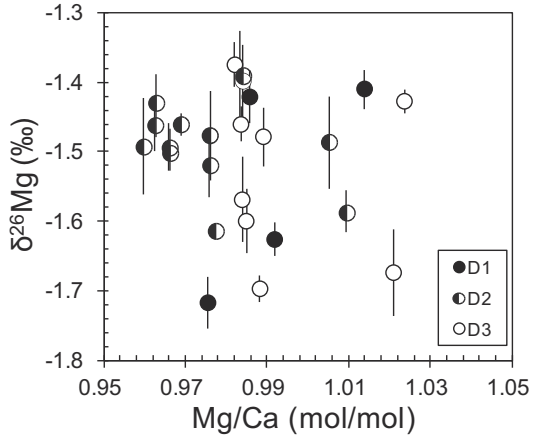

Fig. 4. Cross plot of δ^{26}Mg values versus Mg/Ca molar ratios for three types of dolomites in the Wumishan formation. D1, D2 and D3 represent dolomicrite (<50 μm), sub-euhedral dolomite (50–200 μm) and anhedral dolomite (⩾500 μm), respectively.

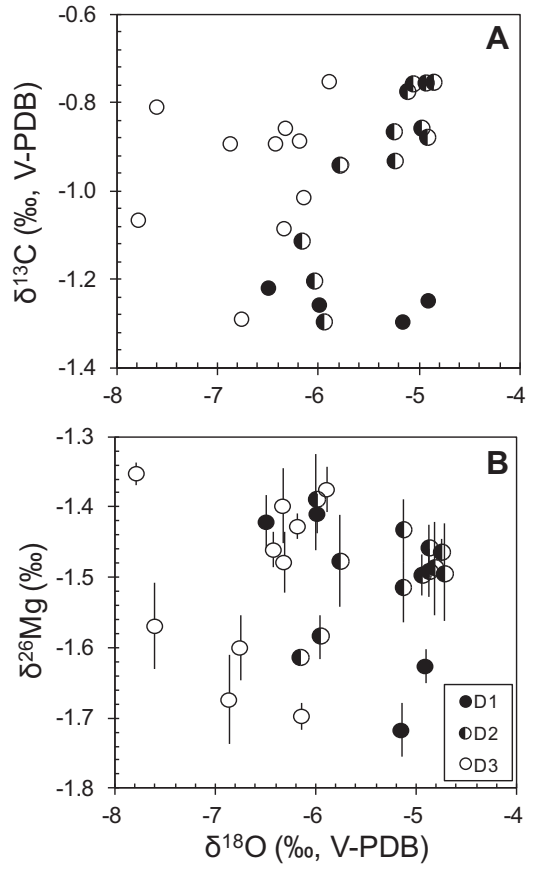

Fig. 5. Cross plots of (A) δ^{13}C and (B) δ^{26}Mg versus δ^{18}O for the Wumishan dolostones. D1, D2 and D3 represent dolomicrite (<50 μm), sub-euhedral dolomite (50–200 μm) and anhedral dolomite (⩾500 μm), respectively.

necessary to evaluate the potential diagenetic alterations of the Wumishan dolostones.

Oxygen isotopes have been widely used as a proxy for the potential diagenetic alterations of carbonate (Xiao et al., 1997), because water–rock interactions would result in significant enrichment in ^{16}O. Relatively high δ^{18}O value (−4‰ to −8‰) and absence of correlation between δ^{13}C and δ^{18}O (Fig. 5A) suggest that the Wumishan dolostones, in general, might have undergone limited degree of diagenetic alteration, and their geochemical signals might have been retained (Kaufman and Knoll, 1995; Xiao et al., 1997). δ^{18}O values of the D3 dolomites are systematically lighter than that of D1 and D2 dolomites, while the D1 and D2 dolomites have similar ranges of δ^{18}O (Fig. 5A). This implies that the D3 dolomite might have undergone more severe diagenetic alterations than the D1 and D2 dolomites. However, lack correlation between δ^{18}O and δ^{26}Mg values for all types of dolomites (Fig. 5B), particularly, similar δ^{26}Mg values of the D3 and D1/D2 dolomites imply that Mg isotopic compositions of the Wumishan dolostones are conservative during diagenesis and might record the pristine values. This is consistent with previous studies on Mg isotopic compositions of ancient dolostones, demonstrating that diagenesis (<200 °C) and low grade metamorphosis (>200 °C) have little impact on Mg isotopic system of dolomite (Geske et al., 2012; Azmy et al., 2013).

5.2. Mg isotope systematics of Mesoproterozoic dolostone

Three lines of evidence indicate that dolomite formation might have been favored in Mesoproterozoic than younger ages (Grotzinger and Knoll, 1995). Firstly, high atmospheric CO_2 level and high seawater alkalinity might have favored carbonate precipitation in Mesoproterozoic (Kaufman and Xiao, 2003; Bartley and Kah, 2004), as evident with abundant sedimentary structures indicating inorganic carbonate precipitation (Morris et al., 1990; Grotzinger and Kasting, 1993; Grotzinger and Knoll, 1995). Furthermore, dolomite formation might have been accelerated in Mesoproterozoic continental margins (Zhang et al., 2012a), where sulfidic conditions might have been pervasive (Canfield, 1998; Reinhard et al., 2013; Lyons et al., 2014). Finally, widespread microbial-induced structures and thrombolites/stromatolites in Mesoproterozoic carbonates suggest that microbes might have played an important role in carbonate precipitation (Grotzinger and Knoll, 1999; Grotzinger et al., 2000; Riding, 2000). Thus, dolomite formation might have been favored in Mesoproterozoic oceans with high alkalinity, H_2S-rich, and widespread microbial activities. This scenario is consistent with more than 90% of successions in the Changchengian and Jixianian Groups consisting of dolostones (Chu et al., 2007).

Although dolomite formation is suggested to be favored in Mesoproterozoic oceans, Mg isotopic compositions of the Wumishan dolostones (−1.72‰ to −1.35‰) are indistinguishable from those of younger dolostones (Fig. 6). If we accept that the formation of massive dolostone in Mesoproterozoic oceans behaved in a manner similar to most marine limestone direct precipitation from seawater (Tucker, 1982; Sibley, 1991; Hood et al., 2011), and Mg isotope fractionation during dolomite formation is ~2.0‰ (Table 2), then δ^{26}Mg value of Mesoproterozoic seawater would vary from ~0.2‰ to ~0.6‰, which is significantly

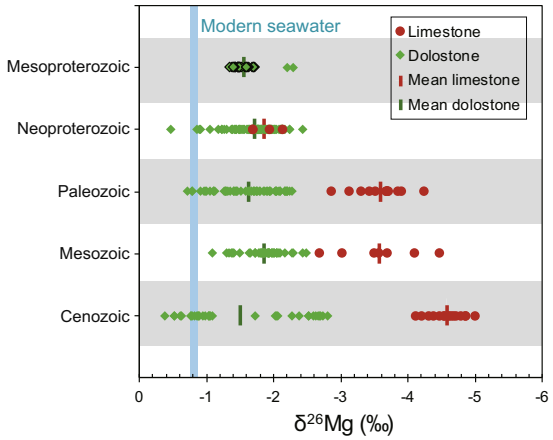

Fig. 6. Compilation of the published δ^{26}Mg data for marine carbonates over geological time. Data are grouped into five bins based on geological era: Mesoproterozoic, Neoproterozoic, Paleozoic, Mesozoic and Cenozoic. Red circles and green diamonds refer to limestone and dolostone, respectively; red and green short bars represent the average composition for limestone and dolostone, respectively. The Mg isotopic data of Cenozoic dolostones are from Higgins and Schrag (2010), Azmy et al. (2013), Fantle and Higgins (2014), and Geske et al. (2015a,b), Mesozoic dolostones are from Galy et al. (2002) and Geske et al. (2012, 2015a), Paleozoic dolostones are from Jacobson et al. (2010), Pokrovsky et al. (2011), Azmy et al. (2013), Lavoie et al. (2014), and Geske et al. (2015a), Neoproterozoic dolostones are from Pokrovsky et al. (2011), Kasemann et al. (2014), and Liu et al. (2014), and Mesoproterozoic dolostones are from Pokrovsky et al. (2011) and this study (green diamonds with black boundary). The data sources of Cenozoic limestone are from Higgins and Schrag (2015), Mesozoic limestones are from Galy et al. (2002) and Buhl et al. (2007), Paleozoic limestones are from Immenhauser et al. (2010) and Azmy et al. (2013), and three data of Neoproterozoic limestones are from Kasemann et al. (2014). (For interpretation of the references to color in this figure legend, the reader is referred to the web version of this article.)

heavier than modern seawater (−0.82‰, Ling et al., 2011). Such heavy Mg isotopic composition of seawater is unlikely because seawater δ^{26}Mg value shows limited variation even though there is a fourfold increase in seawater Mg/Ca over Cenozoic (Higgins and Schrag, 2015). Therefore, Mg isotopic compositions of dolomite might not be simply determined by the δ^{26}Mg value of seawater and isotope fractionation for dolomite formation alone, other factors must be considered. To explain this unexpected observation and further explore the Mg isotopic systematics of dolomite formation, here we apply the one dimensional Diffusion–Advection–Reaction (1D-DAR) model. To simplify the calculation, we assume that Mg for dolomite formation is directly supplied from the overlying contemporaneous seawater and dolomite formation initiates from the water–sediment interface (WSI).

5.3. Diffusion–Advection–Reaction model for dolomite formation

5.3.1. Model description

The 1D-DAR model was designed to quantify the geochemical profiles of sediment pore water (Richter and DePaolo, 1987; Fantle and DePaolo, 2007; Higgins and Schrag, 2010). In this model, three physio-chemical processes are taken into consideration: molecular diffusion, advection, and chemical reaction. In the 1D-DAR model, we assume that contemporaneous seawater is the major source of Mg for dolomite formation, and formation of dolomite takes place under normal marine hydrodynamic conditions. These assumptions are reasonable, because massive dolomite formation with large areal coverage (e.g., the Mesoproterozoic Wumishan dolostone in North China Block) is obviously cannot be explained by any available dolomitization models, which emphasize various specific hydrodynamic conditions (Warren, 2000). Furthermore, seawater can provide sufficient Mg, thus representing the only plausible Mg source for massive dolomite formation (Given and Wilkinson, 1987). However, it should be noted that the 1D-DAR model does not consider the thermodynamic and kinetic aspects of the dolomite formation, i.e., assuming both criteria are already met. Thus, the 1D-DAR model can (1) quantify whether there is enough Mg supply from contemporaneous seawater for complete dolomitization, and (2) simulate the Mg isotopic composition of dolomite/dolostone.

The simplified 1D-DAR model is expressed as:

$$\frac{\partial [C]}{\partial t} = D_z \frac{\partial^2 [C]}{\partial z^2} - s\frac{\partial [C]}{\partial z} - R[C] \quad (1)$$

where $[C]$ is the concentration of a certain element, z is the depth below the WSI, s is the sedimentation rate, D_z is the vertical diffusivity coefficient of bulk sediment (m^2/year), and R is the first-order rate constant for chemical reactions that remove elements from pore water. In this equation, $D_z \frac{\partial^2 [C]}{\partial z^2}$ denotes the effect of molecular diffusion that follows Fick's second law; $-s\frac{\partial [C]}{\partial z}$ describes the effect of pore water advection; and $-R[C]$ is the chemical reaction term quantifying the removal of elements from pore water. To model the Mg isotopic profiles (i.e., δ^{26}Mg) of pore water, we treat isotope ^{24}Mg and ^{26}Mg separately. Eq. (1) can be re-expressed as follows:

$$\frac{\partial [^i\mathrm{Mg}]}{\partial t} = D_{\mathrm{Mg}} \frac{\partial^2 [^i\mathrm{Mg}]}{\partial z^2} - s\frac{\partial [^i\mathrm{Mg}]}{\partial z} - R_{i_{\mathrm{Mg}}}[^i\mathrm{Mg}] \quad (2)$$

where $[^i\mathrm{Mg}]$ is the pore water concentration of ^{24}Mg or ^{26}Mg. D_{Mg} is the same for both ^{24}Mg and ^{26}Mg due to limited fractionation of Mg isotopes during diffusion process ($\alpha^{26/24}_{\mathrm{diffusion}} = 1.00003 \pm 0.00006$ at 75 °C) (Richter et al., 2006). In the reaction term, $R_{i_{\mathrm{Mg}}}$ is the rate of net removal of ^{24}Mg or ^{26}Mg from sediment pore water. In the carbonate deposition system, precipitation of authigenic carbonate minerals is the predominant chemical reaction in the shallow depth of sediment pore water (Scholle et al., 1983; Scoffin, 1987). Here, dolomite formation via replacement of Ca-carbonate is the chemical reaction involved with Mg (Warren, 2000). For simplicity, we assume that dolomite formation takes place immediately below the WSI.

The Mg isotopic fractionation during dolomite formation is reflected by the difference of rate constants between ^{24}Mg and ^{26}Mg. The relationship between the fractionation factor (α^{26}_{24}) and the rate constants can be expressed as:

Table 2
Summary of Mg isotope fractionation between aqueous solution and carbonate minerals ($\Delta^{26}Mg_{aq\text{-}carb}$), including high-Mg calcite, low-Mg calcite, aragonite and dolomite.

Carbonate mineral	Species	Reference	Temperature (°C)	$\Delta^{26}Mg_{aq\text{-}carb}$
Abiogenic calcite		Immenhauser et al. (2010)	10.3 ± 0.5	1.63 ~ 2.24
		Li et al. (2012)	4 ~ 45	2.22 ~ 2.70
		Mavromatis et al. (2013)	25	1.90 ~ 3.20
		Saulnier et al. (2012)	25 ± 0.5	1.49 ~ 2.29
Biogenic high-Mg calcite	Benthic forams	Wombacher et al. (2011), Yoshimura et al. (2011)	1 ~ 23.5	1.86 ~ 2.85
	Coraline red algaes	Hippler et al. (2009), Wombacher et al. (2011)	6 ~ 19	2.15 ~ 2.42
	Echinoids	Hippler et al. (2009), Wombacher et al. (2011)	9.5 ~ 22	1.62 ~ 1.93
	Deep sea corals	Wombacher et al. (2011), Yoshimura et al. (2011)	2.5 ~ 19.5	2.34 ~ 2.63
	Sponges	Wombacher et al. (2011)	24 ~ 27	2.44
Biogenic low-Mg calcite	Planktic forams	Pogge von Strandmann (2008), Wombacher et al. (2011)	20 ~ 30	3.30–4.50
	Bivalves	Hippler et al. (2009)	3.5 ~ 19	2.55–4.25
	Brachiopods	Hippler et al. (2009), Wombacher et al. (2011)	9.5 ~ 12.5	1.05–1.45
	Coccoliths	Ra et al. (2010), Müller et al. (2011), Wombacher et al. (2011)	15 ~ 32.8	0.50–2.20
Abiogenic aragonite		Wang et al. (2012b)	25	0.81 ~ 1.09
Biogenic aragonite	Shallow corals	Hippler et al. (2009),Wombacher et al.(2011), Yoshimura et al.(2011),Planchon et al. (2013), Saenger et al. (2013)	20 ~ 29	0.85–1.20
	Deep sea corals	Wombacher et al. (2011), Saenger et al. (2013)	9 ~ 14.6	0.77–1.00
	Sponges	Wombacher et al. (2011)	16 ~ 28	0.70 ~ 2.30
	Bivalves	Planchon et al. (2013)	15	1.07 ~ 3.4
Dolomite		Higgins and Schrag (2010)	~4	2.00 ~ 2.70
		Rustad et al. (2010)	25	−1.20
		Schauble (2011)	25	3.10
		Fantle and Higgins (2014)	~10	2.00
		Mavromatis et al. (2014)	~10	2.6
		Geske et al. (2015a)	5 ~ 45	−0.10 ~ 0.70
		Li et al. (2015)	130 ~ 220	0.72 ~ 1.11

$$\frac{R_{26_{Mg}}}{R_{24_{Mg}}} = \alpha_{24}^{26} \tag{3}$$

Assuming a steady state with invariant pore water profiles (i.e., $\frac{\partial[C]}{\partial t} = 0$, justification is provided in Appendices) and constant $D_{Mg}, R_{i_{Mg}}$, and s, Eq. (2) becomes an ordinary differential equation, and the solution is given by:

$$[^{i}Mg] = [^{i}Mg]_0 e^{\frac{\left[s-(s^2+4R_{i_{Mg}}D_{Mg})^{1/2}\right]}{2D_{Mg}}\times z} \tag{4}$$

The pore water profiles of ^{24}Mg and ^{26}Mg are calculated separately by Eq. (4), and isotopic composition of pore water ($\delta^{26}Mg_{pw}$) can be calculated by the following equation:

$$\delta^{26}Mg_{pw} = \ln([^{26}Mg]/[^{24}Mg] \times 1000) \tag{5}$$

Eq. (5) is not the traditional expression of delta notation for $\delta^{26}Mg_{pw}$, which requires a standard term (e.g., DSM3). To omit the standard term, the initial $[^{24}Mg]_0$ and $[^{26}Mg]_0$ at the WSI are set to satisfy the following equation:

$$\delta^{26}Mg_{sw} = \ln([^{26}Mg]_0/[^{24}Mg]_0 \times 1000) \tag{6}$$

where $\delta^{26}Mg_{sw}$ is the Mg isotopic composition of seawater, that equals to the Mg isotopic composition of pore water at the WSI. At any depth below the WSI, Mg isotopic composition of instantaneous dolomite formation ($\delta^{26}Mg_{dol}$) can be calculated by:

$$\delta^{26}Mg_{dol} = \delta^{26}Mg_{pw} - \Delta^{26}Mg_{dol} \tag{7}$$

where $\Delta^{26}Mg_{dol}$ is the Mg isotope fractionation between aqueous solution and dolomite. Complete dolomitization (i.e., 100% conversion of Ca-carbonate into dolomite) is a prolonged process beginning at the WSI and terminating at depth where dolomitization is complete.

Accordingly, Mg isotopic compositions of dolomite change continuously throughout the whole dolomitization process. To calculate Mg isotopic composition of instantaneous dolomite formation at each sediment depth, we divide sediment into depth slices, and add up from the top slice at the WSI ($z = 0$) to the last slice in which dolomitization completes. The Mg isotopic composition of bulk dolomite (i.e., dolostone, $\delta^{26}Mg_{dst}$) at depth z can be calculated as following:

$$\delta^{26}Mg_{dst} = \frac{\sum_0^i(\delta^{26}Mg_{dol} \times [Mg]^i)}{\sum_0^i [Mg]^i} \tag{8}$$

where i is the index of depth slice, and the depth (z) of the slice i can be calculated as $z = i \times h$, where h is the thickness of each slice. The amount of Mg being transferred from pore water to dolomite is determined by the reaction rate of dolomite formation, sedimentation rate, and Mg concentration of pore water. The amount of Mg (M^i) being transferred from pore water to dolomite at depth slice i, and the cumulative amount of Mg from the WSI to depth slice i can be expressed by Eqs. (9) and (10), respectively:

$$M^i = [Mg]^i \times R \times \frac{h}{s} \tag{9}$$

$$M^z = \sum_0^i M^i = \sum_0^i \left([Mg]^i \times R \times \frac{h}{s}\right) \tag{10}$$

To estimate the depth of complete dolomitization, we assume that the precursor minerals are calcite containing 5 mol.% of $MgCO_3$. In the top 100 m, the porosity of calcareous sediments normally ranges from 50% to 70% (Tucker and Wright, 1990). Assuming sediment porosity of 60%, 1 cubic decimeter of stoichiometric dolomite formation (Mg/Ca = 1, density = 2.5 g/cm^3, porosity = 20%) requires ~10 mol of Mg, which equals to ~17 mol of Mg from per liter of pore water, which is the cutoff for the complete dolomitization.

5.3.2. Parameter setup

To quantify whether there is enough Mg supply from seawater for complete dolomitization by using the 1D-DAR model, the following parameters need to be determined: $D_{Mg}, s, R_{i_{Mg}}$, and $[Mg]_0$.

D_{Mg} is the diffusivity coefficient in sediments, and can be calculated by the following equation (Li and Gregory, 1974):

$$D_{Mg} = D_{sw}/(1 - \ln(\phi^2)), \tag{11}$$

where ϕ is the porosity of sediment, D_{sw} is the diffusivity coefficient of Mg in sea water, which is temperature dependent, and varies between 3.26×10^{-6} cm^2/s and 6.55×10^{-6} cm^2/s from 0 °C to 25 °C (Schulz and Zabel, 2006). At the same temperature range, D_{Mg} varies from 1.61×10^{-6} cm^2/s to 3.34×10^{-6} cm^2/s at a constant porosity of 60%. We here choose 2.5×10^{-6} cm^2/s as a preferred parameter. Because depth of dolomite formation is relatively shallow, we can assume the sediment porosity to be constant.

The sedimentation rate of normal marine non-reef carbonate varies from 1 cm/ky to 10 cm/ky (Tucker and Wright, 1990). Here, we chose the sedimentation rate (s) of 5 cm/ky (i.e., 0.00005 m/year) as a preferred parameter. Modern seawater $[Mg]_0$ is ~53 mM, but this value might be higher during the Proterozoic (Holland et al., 1986). An estimate of 100 mM seawater [Mg] in the Precambrian oceans has been proposed by Hardie (1996). We thus use seawater [Mg] of 100 mM in our model.

Reaction rate for dolomite formation within pore water is difficult to constrain. In the modern marine calcareous settings, R_{Mg} ranges from $<10^{-7}$/year to 10^{-4}/year, indicating extremely low rate for authigenic carbonate formation (Higgins and Schrag, 2010). This suggests that little dolomite formation in modern marine sediments, in addition to the kinetic problem, can be attributed, at least partially, to the insufficient supply of Mg from seawater (Mazzullo, 2000). In order to provide enough Mg for pure dolomite formation, R_{Mg} should range from 0.01/year to 0.001/year, which means 1 l of pore water can provide 1 mol Mg for dolomite formation at the WSI for every 1000–10,000 years.

In addition to the above parameters, as shown in Eq. (3), Mg isotopic system for dolomite formation is also related to Mg isotopic composition of seawater ($\delta^{26}Mg_{sw}$) and the isotope fractionation between dolomite and pore

water ($\Delta^{26}Mg_{dol}$). There is no constraint on the $\delta^{26}Mg_{sw}$ values in the Mesoproterozoic so far, although heavier Mg isotopic composition of seawater is inferred from abundant dolomite formation in Mesoproterozoic as mentioned early. In our model, we set the default $\delta^{26}Mg_{sw}$ value of −0.5‰, slightly heavier than modern seawater of −0.82‰ (Ling et al., 2011). Although direct measurement of Mg isotopic fractionation for dolomite precipitation at low-temperature is unrealizable so far, some constrains on $\Delta^{26}Mg_{dol}$ by theoretical calculations (Rustad et al., 2010; Schauble, 2011) and marine sediment and related pore water profiles (Higgins and Schrag, 2010; Fantle and Higgins, 2014; Mavromatis et al., 2014) are estimated to be 2.0 ~ 3.0‰ with temperature varying from 4 °C to 25 °C (Table 2). These estimations are consistent with the function relationship between temperature (T) and $\Delta^{26}Mg_{dol}$, i.e., $\Delta^{26}Mg_{dol} = 0.1554(\pm0.0096) \times 10^6/T^2$, obtained from high-temperature dolomite precipitation experiments (Li et al., 2015). In the modeling, we run several scenarios by keeping $\Delta^{26}Mg_{dol}$ within the range between 1.75‰ and 2.08‰, corresponding to the reaction temperature varying between 25 °C and 0 °C. And the fractionation of 1.94‰ for dolomite formation at 10 °C is chosen as a default parameter.

To test the sensitivity of the modeling parameters, we initiate with the default values and sequentially modify each single parameter. Both dolomite content and $\delta^{26}Mg_{dst}$ value are simulated in each run.

5.3.3. Modeling results

The profiles of Mg concentration of pore water and $\delta^{26}Mg_{dst}$ simulated by the 1D-DAR model are shown in Fig. 7. As discussed above, complete dolomitization is set to the depth, where ~17 mol Mg has been transferred from 1 l of pore water into dolomite. Below this depth, although Mg extraction from pore water still continues, dolomite formation becomes negligible in reality. If we use the aforementioned parameters ($D_{Mg} = 2.5 \times 10^{-10}$ m^2/s, $s = 5$ cm/ky, $R_{Mg} = 0.01$/year, $[Mg]_0 = 100$ mM, $\delta^{26}Mg_{sw} = -0.5$‰ and $\Delta^{26}Mg_{dol} = 1.94$‰, $h = 1$ cm) and assume that dolomite formation initiates at the WSI, complete dolomitization occurs at ~2.87 m below the WSI, which is equivalent to ~57.4 ky after deposition. The 1D-DAR modeling results also show that Mg isotopic composition of the earliest dolomite precipitation at the WSI and the mature dolomite at depth with complete dolomitization are −2.44‰ and −1.59‰, respectively (Fig. 7B).

5.4. Controls and Mg isotope systematics of dolomite formation

As shown in the 1D-DAR model, dolomite formation is controlled by various factors. We discuss below how variation of individual parameter affects the Mg content and Mg isotopic systematics of dolomite formation.

5.4.1. Seawater Mg concentration ($[Mg]_0$)

The 1D-DAR model indicates that with the higher $[Mg]_0$ favors dolomite formation (Fig. 7A). When $[Mg]_0$ is 50 mM of the modern seawater value (Carpenter and Manella, 1973), regardless of the reaction rate, complete dolomitization cannot be achieved due to insufficient supply of Mg from contemporaneous seawater (Fig. 7A). In contrast, increase in $[Mg]_0$ to 150 mM causes earlier completion of dolomitization at shallower depth below the WSI (~0.91 m). Although Mg isotopic profiles of dolomite are independent of $[Mg]_0$, earlier formation of dolostone at shallower depth would cause about 0.4‰ decrease in $\delta^{26}Mg_{dst}$ from −1.46‰ to −1.87‰ (Fig. 7B). The modeling result is inconsistent with some traditional models (e.g., the Coorong model and the seawater-freshwater mixing zone model) that seawater dilution (decrease in $[Mg]_0$) favors dolomite precipitation (Hanshaw et al., 1971; Rosen et al., 1989). Such discrepancy reflects the complexity of dolomite formation, which is controlled by both the supply of Mg and the reaction kinetics (e.g., overcome the kinetic barrier imposed by the hydration of seawater Mg^{2+} (Land, 1998)).

5.4.2. Sedimentation rate

Sedimentation rate is the key control on the advection term in the 1D-DAR model (Schulz and Zabel, 2006). According to the 1D-DAR model, sedimentation rate determines the retention time of sediments at certain depth interval. When sedimentation rate is high, rapid burial would result in insufficient supply of Mg for dolomitization, and vice versa. As shown in Fig. 7C, complete dolomitization occurs at ~20 cm below the WSI if the sedimentation rate is extremely slow (e.g., 1 cm/ky), implying it takes ~20 ky to complete dolomitization. This is about three times faster than the dolostone formation in settings with sedimentation rate of 5 cm/ky. Consequently, Mg isotopic composition of dolostone formed at lower sedimentation rate of 1 cm/ky (−2.33‰) is lighter than that formed at sedimentation rate of 5 cm/ky (−1.59‰) (Fig. 7D). In contrast, incomplete dolomitization would be taken place at higher sedimentation rate of 10 cm/ky, and dolostone has heavier $\delta^{26}Mg$ value of −1.49‰.

5.4.3. Temperature

Although temperature is not shown in the 1D-DAR model Eq. (1), both diffusion coefficient (D_{Mg}) and Mg isotope fractionation during dolomite formation ($\Delta^{26}Mg_{dol}$) are temperature dependent (Li and Gregory, 1974; Li et al., 2015). In this section, we focus on the effects of temperature on D_{Mg}, and variation of $\Delta^{26}Mg_{dol}$ on the content and Mg isotopic systematics of dolomite formation will be discussed in Section 5.4.6. According to the Arrhenius function, $D_{Mg} = D_0 e^{(-E_a/RT)}$ (E_a is the activation energy, R is the gas constant, and T is temperature in Kelvin (Hoefs, 2009)), D_{Mg} would increase by a factor of two when temperature raises from 0 °C to 25 °C (Boudreau, 2011). Therefore, increase of temperature is in favor of seawater Mg^{2+} diffusion into the sediment column, resulting in complete dolomitization at shallower depth below the WSI (Fig. 7E). Conversely, increase in D_{Mg} as elevating temperature would cause decrease in $\delta^{26}Mg_{dst}$. For example, at a constant $\Delta^{26}Mg_{dol}$ of 1.94‰, $\delta^{26}Mg$ of dolostone formed

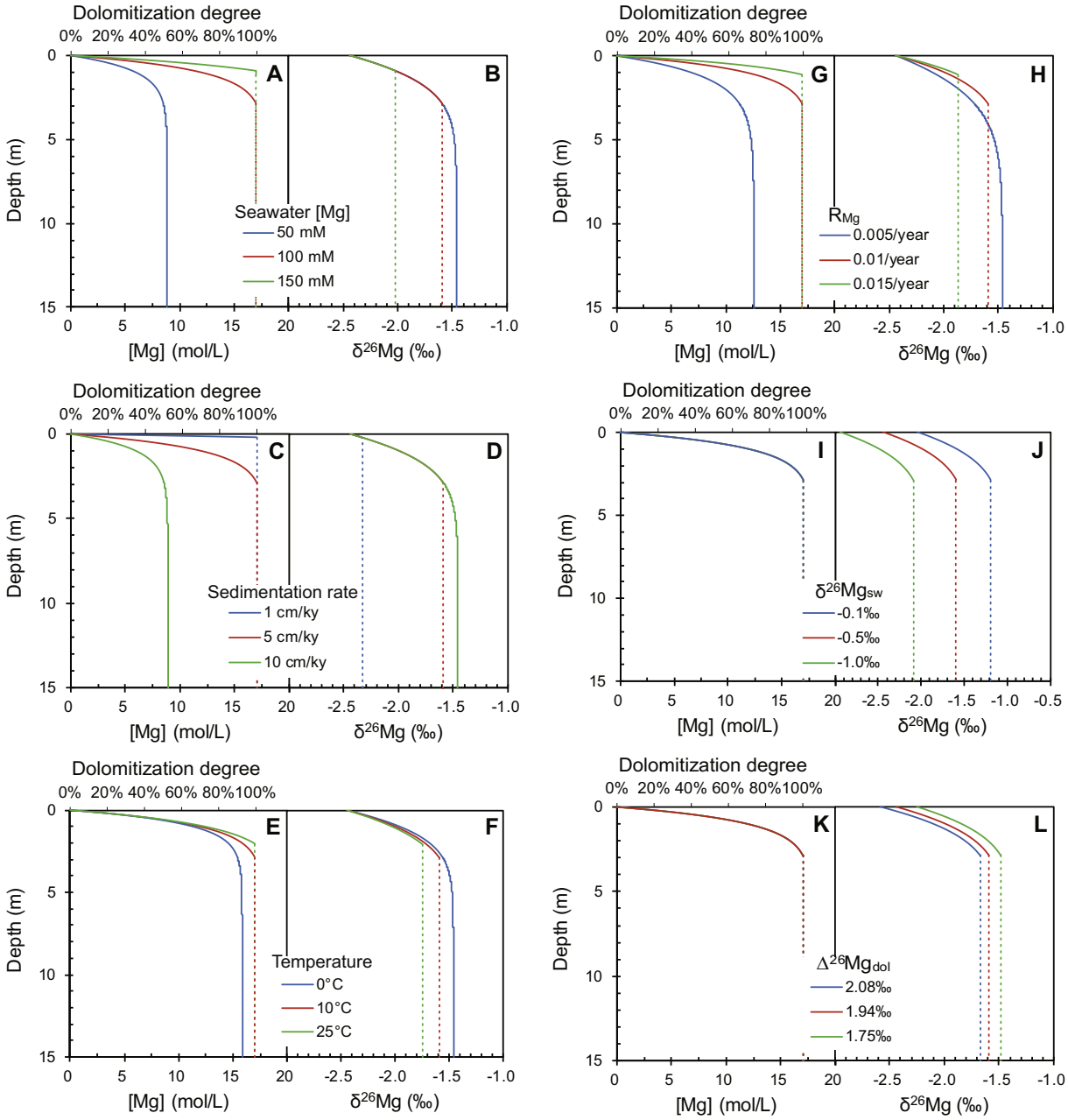

Fig. 7. The 1D-DAR modeling results showing the depth profiles of both cumulative Mg transferred from pore water to dolostone (lower *x*-axis in the left panel), degree of dolomitization (upper *x*-axis in the left panel), and δ^{26}Mg of dolostones (right panel). The following controls on dolomite formation and Mg isotopic compositions of dolostones are shown: seawater Mg concentration [(A) and (B)]; sedimentation rate [(C) and (D)]; temperature [(E) and (F)]; rate of dolomite formation [(G) and (H)], seawater δ^{26}Mg [(I) and (J)], and Mg isotope fractionation for dolomite formation. Red line is our preferred model for formation of dolomites in the Wumishan Formation. Blue and green lines represent model runs where we considered variations in boundary condition (i.e., the sensitivity tests of the model results). (For interpretation of the references to color in this figure legend, the reader is referred to the web version of this article.)

at 10 °C is about 0.2‰ heavier than that formed at 25 °C (Fig. 7F).

5.4.4. Rate of dolomite formation

Dolomite formation within sediments is the primary driving force for seawater Mg diffusion into sediment column (Whitaker et al., 2004). In the 1D-DAR model, Mg supply from seawater is very sensitive to the reaction rate constant (R_{Mg}). In order to complete dolomitization, R_{Mg} needs to be about two orders of magnitude higher than the upper bound of the present day level (Higgins and Schrag, 2010). Increase in R_{Mg} might relate to the thermodynamic and kinetic issues during dolomite formation, such as activity of pore water Mg^{2+}, alkalinity, and degree of

saturation (Mazzullo, 2000). As shown in the 1D-DAR model, increase in R_{Mg} by 50% would result in complete dolomitization at shallower depth of 1.12 m below the WSI with respect to complete dolomitization under the default condition (0.01/year) (Fig. 7G). Similarly, increase in R_{Mg} from 0.01/year to 0.015/year would lead to around 0.3‰ decrease in $\delta^{26}Mg_{dst}$ (Fig. 7H). On the other hand, decrease in R_{Mg} by a factor of two (from 0.01/year to 0.005/year) would end up with incomplete dolomitization with higher $\delta^{26}Mg_{dst}$ value of −1.47‰ (Fig. 7H).

5.4.5. Seawater Mg isotopic composition ($\delta^{26}Mg_{sw}$)

Although $\delta^{26}Mg_{sw}$ is not included in the 1D-DAR model, $\delta^{26}Mg_{dst}$ is certainly affected by $\delta^{26}Mg_{sw}$ as shown in Eq. (6). Modern seawater has homogeneous $\delta^{26}Mg$ value of −0.82‰ (Foster et al., 2010; Ling et al., 2011). However, Mg isotopic composition of seawater over the geological past might have been fluctuated, although there is no reliable record of the seawater $\delta^{26}Mg$ value so far. Downcore fluctuations in $\delta^{26}Mg$ values of bulk pelagic sediments in excess of 1.5‰ are reported by Higgins and Schrag (2012), suggesting the potential variation in seawater $\delta^{26}Mg$ over the Neogene. Moreover, Pogge von Strandmann et al. (2014) propose the gradual increase in $\delta^{26}Mg_{sw}$ from the present value of −0.82‰ to ~0‰ at 15 Ma based on foraminifera record. In contrast, a study on pelagic carbonate sediments demonstrates limited variation in $\delta^{26}Mg_{sw}$ in the past 70 Ma (Higgins and Schrag, 2015). Here, we chose three different $\delta^{26}Mg_{sw}$ values (−1.0‰, −0.5‰, and −0.1‰) to test its effect on the Mg isotopic systematics of dolomite formation. The 1D-DAR modeling results show that the degree of dolomitization is not changed with variation in $\delta^{26}Mg_{sw}$ (Fig. 7I). However, change in $\delta^{26}Mg_{sw}$ has an important influence on $\delta^{26}Mg_{dst}$, that Mg isotopic profile of dolostone shifts leftward with decrease in $\delta^{26}Mg_{sw}$ with the same magnitude, and vice versa (Fig. 7J).

5.4.6. Isotope fractionation

Fractionation of Mg isotopes has limited influence on the degree of dolomitization (Fig. 7K), but it directly determines Mg isotopic composition of dolostone formation. As shown in Fig. 7L, increase of $\Delta^{26}Mg_{dol}$ from 1.75‰ to 2.08‰ would results in decrease of $\delta^{26}Mg_{dst}$ from −1.49‰ to −1.67‰, suggesting that the magnitude of variation in $\delta^{26}Mg_{dst}$ is about half of the fluctuation of $\Delta^{26}Mg_{dol}$. In other words, the cumulative Mg isotopic fractionation for dolostone formation ($\Delta^{26}Mg_{dst} = \delta^{26}Mg_{sw} - \delta^{26}Mg_{dst}$) would be smaller than the instantaneous fractionation ($\Delta^{26}Mg_{dol} = \delta^{26}Mg_{pw} - \delta^{26}Mg_{dol}$) (Fig. 8).

5.5. Implications for Mg isotopic systematics of carbonates

Compilation of published Mg isotopic data of marine carbonates reveals the following two observations (Fig. 6): (1) dolostones ($\delta^{26}Mg_{dst}$ = −0.40‰ to −2.80‰) are isotopically heavier than limestones ($\delta^{26}Mg_{lst}$ = −2.70‰ to −5.10‰, with exception of three discrete data set in the Neoproterozoic); and (2) dolostones in different geological period have generally overlapping range of $\delta^{26}Mg_{dst}$, whereas $\delta^{26}Mg_{lst}$ is considerably more variable and changes through time (Fig. 6). The differences between the Mg isotopic systematics of limestones and dolostones cannot be simply ascribed to their crystal structure (Schauble, 2004), because Mg in both calcite and dolomite is in the octahedral coordination (Rustad et al., 2010; Schauble, 2011). Furthermore, dolomite and calcite have similar mean Mg–O bond length of 2.08 Å and 2.12 Å (Finch and Allison, 2007; Schauble, 2011), suggesting that the bond length is not likely to cause such Mg isotopic difference between dolostones and limestones even if isotopic fractionation might be affected by the bond lengths (Li et al., 2014). Instead, we suggest that the systematic difference between limestone and dolostone might be resulted from the distinct precipitation processes for these two types of carbonates.

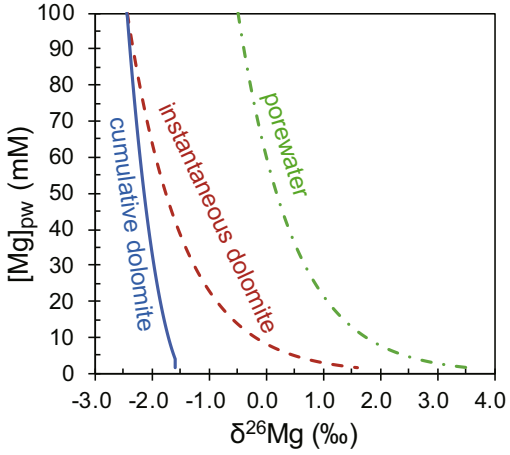

Fig. 8. Comparison of $\delta^{26}Mg$ values of pore water, instantaneous dolomite formation, and cumulative dolomite (i.e., dolostone) formation based on the 1D-DAR model by using the boundary conditions as preferred parameters ($D_{Mg} = 2.5 \times 10^{-10}$ m^2/s, s = 5 cm/ky, R_{Mg} = 0.01/year, $[Mg]_0$ = 100 mM, $\delta^{26}Mg_{SW}$ = −0.5‰ and $\Delta^{26}Mg_{dol}$ = 1.94‰).

Most marine limestone is precipitated from seawater either inorganically or biologically (Scoffin, 1987). As a minor element, Mg is directly sourced from seawater and replaces Ca in the crystal lattice of Ca-carbonate minerals (Mucci and Morse, 1983). Thus, the isotopic composition of limestone ($\delta^{26}Mg_{lst}$) can be expressed by the following equation:

$$\delta^{26}Mg_{lst} = \delta^{26}Mg_{sw} - \Delta^{26}Mg_{lst} \quad (12)$$

where $\delta^{26}Mg_{lst}$ is the Mg isotope fractionation during limestone precipitation.

In contrast, dolostone formation normally occurs within sediments, and Mg in dolostone is derived from pore water. Dolostone formation is considered as a consecutive process within sediments in order to uptake enough Mg from seawater for dolomitization (Whitaker et al., 2004). Mg isotopic composition of instantaneous dolomite formation ($\delta^{26}Mg_{dol}$) at certain depth is calculated by Eq. (7). As

indicated by the 1D-DAR model, $\delta^{26}Mg_{pw}$ becomes progressively heavy through sediment depth by removal of light Mg isotopes into dolomite. Therefore, dolomite formed at deeper depth below the WSI would be more enriched in ^{26}Mg than that formed at shallower depth of sediments, suggesting that isotopic composition of dolostone ($\delta^{26}Mg_{dst}$, calculated by Eq. (8)) is always heavier than $\delta^{26}Mg_{dol}$ at the WSI (Fig. 8).

Assuming calcite and dolomite precipitations have the same isotope fractionation of ~1.94‰, as shown in the 1D-DAR model, the maximum difference between limestone and dolostone is ~0.85‰ (i.e., $\delta^{26}Mg_{dst} - \delta^{26}Mg_{lst} \leqslant 0.85‰$) (Fig. 7L). This value is smaller than the isotopic difference between Phanerozoic limestones and dolostones (Fig. 6). This discrepancy may be ascribed to relatively larger Mg isotopic fractionation for Phanerozoic limestones ($\Delta^{26}Mg_{lst}$) compared to the canonical fractionation for inorganic calcite precipitation (~1.94‰) used in the 1D-DAR model. In fact, biogenic Ca-carbonate is the major source of marine limestone in Phanerozoic oceans (Boss and Wilkinson, 1991), and carbonate-secreting organisms can fractionate Mg isotopes up to 4.5‰ (Wombacher et al., 2011) (Table 2).

Another observation from the limestone–dolostone compilation data is that dolostones in different geological period have an overlapping range of variation in $\delta^{26}Mg_{dst}$ (Fig. 6). In contrast, $\delta^{26}Mg_{lst}$ has a wider range of variation, particularly for Phanerozoic samples. This may result from the following two reasons. First, the range of $\Delta^{26}Mg_{dol}$ might be smaller than fluctuation of $\Delta^{26}Mg_{lst}$ (Table 2). Current estimation of $\Delta^{26}Mg_{dol}$ at low-temperature by natural system investigations ranges from 2‰ to 2.7‰ (Higgins and Schrag, 2010; Fantle and Higgins, 2014; Mavromatis et al., 2014), whereas $\Delta^{26}Mg_{calcite}$ varies between 0.5‰ and 4.5‰ (Ref. Saenger and Wang, 2014). Second, as shown in the 1D-DAR model, the Mg isotopic fractionation for dolostone ($\Delta^{26}Mg_{dst}$) is only half of $\Delta^{26}Mg_{dol}$ (Fig. 7J), further shrinking the variation of $\delta^{26}Mg_{dst}$.

Finally, current data compilation indicates that there is >1‰ decrease in the average $\delta^{26}Mg_{lst}$ from the Mesozoic to Cenozoic, while Paleozoic and Mesozoic limestones have nearly identical average $\delta^{26}Mg_{lst}$ (Fig. 6). It is unclear whether such differences indicate a secular variation in $\delta^{26}Mg$ of seawater in the geological history or reflect sorts of sampling bias due to relatively small data set at current stage.

5.6. Using Mg isotopes to constrain dolostone formation

Dolostones of different ages with overlapping range of Mg isotopic composition (Fig. 6) and absence of systematic difference among different types of dolomite (Geske et al., 2012, 2015a) imply that using Mg isotope to constrain dolomite formation is not straightforward. This is supported by the 1D-DAR modeling results that Mg isotopic systematics of dolostone formation is sensitive to many factors, including seawater Mg concentration, sedimentation rate, temperature, dolomite formation rate, seawater $\delta^{26}Mg$ value and isotopic fractionation (Fig. 7).

Absence of systematic difference among different types/ages of dolomite might result from the following reasons. First, the DAR model can only be applied to certain dolomitization process, in which Mg is supplied by diffusion, while dolomite formation with Mg supply from advective fluid flow (e.g., the reflux dolomitization model, Adams and Rhodes, 1960) cannot be simulated by the 1D-DAR model. Furthermore, there is diverse Mg source for dolomitization with a wide range of isotopic compositions (Ref. Li et al., 2012; Geske et al., 2015a), further making Mg isotopic systematic more complicate. Finally, post-dolomitization alterations, such as recrystallization or neomorphism, would alter the texture of dolomite while the Mg isotopic signals remain intact (Geske et al., 2012; Azmy et al., 2013) as evident by the invariant $\delta^{26}Mg$ values among D1, D2 and D3 dolomites in the Wumishan dolostones.

Nevertheless, there is one general rule for dolomite formation that can be drawn from the 1D-DAR model. Regardless of parameter selection, all 1D-DAR modeling results indicate that early-formed dolomite (i.e., complete dolomitization at shallower depth below the WSI) would always be isotopically lighter than late dolomite formation at deeper depth below the WSI (Fig. 7). We suggest that this general rule based on the 1D-DAR model can be applied to explain the variation in $\delta^{26}Mg$ values of some dolomite beds from modern deep sea sediments. For instance, within the similar depth ranges, dolomites within deep sea sediments from ODP site 1082 have heavier $\delta^{26}Mg$ values (−1.72‰ to −2.06‰) than those from ODP site 1012 (−2.38‰ to −2.52‰) (Higgins and Schrag, 2010). Dolomite with heavier Mg isotopic composition has been interpreted as formation of dolomite in a more closed system (e.g., ODP site 1082) (Fantle and Higgins, 2014). In the context of the 1D-DAR model, formation of dolomite in ODP site 1082 might be slower due to relatively lower reaction rate (10^{-6} to 10^{-5} mol Mg/m^3/yr), resulting in dolomite formed at deeper depth below the WSI, where pore water has relatively higher $\delta^{26}Mg$ values. In consequence, removal of Mg from isotopically heavier pore water into dolomite may contribute to heavier $\delta^{26}Mg$ values of dolomites in deep sea sediments from ODP site 1082. In contrast, relatively higher reaction rate (10^{-5} to 10^{-4} mol Mg/m^3/year) in ODP site 1012 may lead to complete dolomitization at shallower depth below the WSI, where pore water and dolomite formation would have relatively lower $\delta^{26}Mg$ values.

6. CONCLUSIONS

Dolostone formation in Mesoproterozoic oceans is believed to be favored and have different origin from those formed in younger oceans. However, Mg isotopic compositions of dolostones from the Mesoproterozoic Wumishan Formation presented here range from −1.35‰ to −1.72‰, which overlaps the range of Mg isotopic variation for dolostone of different ages and is indistinguishable from those of younger Neoproterozoic and Phanerozoic

dolostones. In this study, the 1D-DAR model is applied to explain this unexpected observation and further understand the Mg isotopic systematics for dolomite formation. This model can quantify the amount of dolomite formation and the Mg isotopic composition of dolomite by assuming contemporaneous seawater as the Mg source for dolostone formation. The 1D-DAR modeling results indicate that dolostones have limited range of variation in $\delta^{26}Mg$ compared to limestones, which may be attributed to the limited variation in $\Delta^{26}Mg_{dol}$ and shrinkage in fractionation during dolostone formation. Furthermore, the 1D-DAR model also predicts that dolostone is always isotopically heavier than contemporaneous limestone, which is consistent with the current compilation of Mg isotope data for dolostone and limestone. Finally, the 1D-DAR modeling results suggest that early-formed dolostone at shallower depth below the WSI is isotopically lighter than late-formed dolostone within deeper sediments, suggesting the potential implication of Mg isotopes to constrain the origin of dolostone. This general rule in the context of the 1D-DAR model could be applied to explain variation in Mg isotopic composition of dolomite beds from modern deep sea sediments.

ACKNOWLEDGEMENT

We thank Professor Jia-Wei Chen and Ms. Hong Qin for ICP-OES analysis, and Zhen Yan for stimulating discussions. The manuscript was significantly improved by the constructive reviews from John Higgins, Edward T. Tipper, and one anonymous reviewer. The efficient editorial handling of Fang-Zhen Teng is greatly appreciated. This study is supported by the Natural Science Foundation of China (41272017 and 41322021) for B. Shen and the China Postdoctoral Science Foundation (2014M55006) for K.-J. Huang.

APPENDIX .

A. Justification to use steady state approximation

The exact solution to Eq. (1) in its dimensionless form is given by:

$$C(z,t)=\frac{1}{2}e^{(\frac{s}{2D}-\sqrt{\frac{s^2}{4D^2}+\frac{R}{D}})z}\left\{1+\mathrm{erf}\left(\frac{-z+\sqrt{s^2+4RDt}}{2\sqrt{Dt}}\right)+e^{2\sqrt{\frac{s^2}{4D^2}+\frac{R}{D}}z}\left[1-\mathrm{erf}\left(\frac{-z+\sqrt{s^2+4RDt}}{2\sqrt{Dt}}\right)\right]\right\}, \quad (A.1)$$

where $\mathrm{erf}(x)$ is the error function. We can use this profile to obtain a more accurate expression for Eqs. (9) and (10) for possible complete dolomitization in the original Proterozoic seawater. Using the same logic following Eqs. (9) and (10), we can replace t as z/s, so it measures the time when the layer of sediment reaches depth z. This way, the integration for total amount of reacted Mg is given by integration from depth 0 to some distance where the cutoff of 17 mol/L is reached. For the boundary condition of 100 mM/L, this non-dimensional number is 170.

Consider the baseline case of $s = 5$ cm/ky, $D = 2.5 \times 10^{-10}$ m^2/s, $R = 0.01$/year, complete dolomitization occurs at ~2.7 m, same as that computed from the steady state profile.

In fact, there are two inherent time scales competing when considering the exact solution: the time it takes for C to reach the steady state, and the time to reach complete dolomitization. Based on the parameters of interest, the steady state profile is reached in just a few hundred years, yet complete dolomitization occurs in several to tens of thousands years. As such, the steady state profile of C is a justifiable approximation to estimate the occurrence of complete dolomitization, as far as the parameter range of interest is concerned.

In order for the transient profile Eq. (A.1) to be of relevance, one needs the time scale for C to reach its steady state to be much slower and comparable to the time scale of complete dolomitization. A few directions have been taken as tests. Firstly, decreasing R does lead to slowing down for C to asymptote; however, it makes complete dolomitization impossible. For example, other parameters fixed, at $R = 10^{-7}$/year, the lower bound on present day reaction rate, integration towards $z = \infty$ for the steady profile leads to total reacted Mg of 125 mM/L, yet using transient profile leads to reacted Mg of 106 mM/L. Secondly, decreasing D also leads to slowing down for C to asymptote; however, it also makes complete dolomitization impossible. For example, at $D = 2.5 \times 10^{-15}$ m^2/s, integration towards $z = \infty$ for the steady profile leads to total reacted Mg of 111 mM/L, yet using transient profile leads to reacted Mg of 86 mM/L. Thirdly, increasing s again slows down C to asymptote; yet it again leads to incomplete dolomitization. For example, at $s = 50$ m/ky, integration towards $z = \infty$ for the steady profile leads to total reacted Mg of 103 mM/L, yet using transient profile leads to reacted Mg of 67 mM/L. The final direction is to increase boundary condition at $z = 0$. However, even with boundary condition of an unrealistic 17 mol/L, there is no significant difference between the steady state and the transient as far as the total amount of reacted Mg is of concern. As such, we conclude that within reasonable parameter range, steady state solution is a valid approximation for computation of complete dolomitization.

B. Full solution to the DAR problem

We normalized the DAR Eq. (1) and rewrite as follows:

$$C_t = DC_{zz} - sC_z - RC,$$

$$C(z=0,t) = 1, C(z>0, t=0) = 0. \tag{B.1}$$

Let

$$C(z,t) = v(z,t)e^{-\left(\frac{s^2}{4D}+R\right)t+\frac{s}{2D}z}, \tag{B.2}$$

the governing equation becomes

$$v_t = Dv_{zz},$$

$$v(z=0,t) = e^{Kt}, v(z>0, t=0) = 0 \tag{B.3}$$

where $K = s^2/4D + R$, and the equation can be solved using integral transform.Using Fourier sine transform with $v_s \equiv \int_0^\infty v(z,t)\sin pzdz$, we obtain:

$$-p^2 v_s(p;t) + pv(0,t) = \frac{1}{D}\frac{d}{dt}v_s(p;t), \tag{B.4}$$

so

$$\frac{d}{dt}v_s + Dp^2 v_s = Dpe^{Kt}, v_s(p;0) = \int_0^\infty v(z,0)\sin pzdz = 0 \tag{B.5}$$

The solution to this ordinary differential equation is:

$$v_s = \frac{Dp}{K+Dp^2}\left(e^{Kt} - e^{-Dp^2 t}\right). \tag{B.6}$$

Applying inverse transform, the solution to v is:

$$v = \frac{2}{\pi}\int_0^\infty \frac{Dp}{K+Dp^2}\left(e^{Kt} - e^{-Dp^2 t}\right)\sin pzdp. \tag{B.7}$$

Consider some constant $\tau < 0$,

$$\int_0^\infty e^{\tau z}\sin pzdz = \frac{p}{\tau^2 + p^2}, \tag{B.8}$$

Thus the inverse transform for the first term leads to:

$$\frac{2}{\pi}\int_0^\infty \frac{Dp}{K+Dp^2}e^{Kt}\sin pzdz = e^{Kt-\sqrt{\frac{K}{D}}z}. \tag{B.9}$$

Multiplying the factor $e^{-\left(\frac{s^2}{4D}+R\right)t+\frac{s}{2D}z}$, this portion of the solution leads to $e^{\left(\frac{s}{2D}-\sqrt{\frac{s^2}{4D^2}+\frac{R}{D}}\right)z}$, which is the steady state solution.To obtain the inverse transform for the second term, we recall that:

$$\frac{2}{\pi}\int_0^\infty \frac{Dp}{K+Dp^2}e^{-Dp^2 t}\sin pzdp = \frac{2}{\pi}\int_0^\infty\int_0^\infty e^{-\sqrt{\frac{K}{D}}z'}\sin pz'dz'e^{-Dp^2 t}\sin pzdp. \tag{B.10}$$

Swapping the order of integration and integrate with respect to p, we obtain that

$$\frac{2}{\pi}\int_0^\infty \frac{Dp}{K+Dp^2}e^{-Dp^2 t}\sin pzdp = \int_0^\infty \frac{1}{2\sqrt{\pi Dt}}\left[e^{-\frac{(z'-z)^2}{4Dt}} - e^{-\frac{(z'+z)^2}{4Dt}}\right]e^{-\sqrt{\frac{K}{D}}z'}dz'. \tag{B.11}$$

This is the convolution of an exponential profile with the heat kernel centered at z and $-z$. The one centered at $-z$ is an image of the infinite heat problem centered at z so the summation cancels out at $z = 0$. Multiplying the factor $e^{-\left(\frac{s^2}{4D}+R\right)t+\frac{s}{2D}z}$ and include the steady solution, also simplify the convolution by error function, the final expression for the exact solution to the DAR equation is:

$$C(z,t) = \frac{1}{2}e^{\left(\frac{s}{2D}-\sqrt{\frac{s^2}{4D^2}+\frac{R}{D}}\right)z}\left\{1+\operatorname{erf}\left(\frac{-z+\sqrt{s^2+4RDt}}{2\sqrt{Dt}}\right) + e^{2\sqrt{\frac{s^2}{4D^2}+\frac{R}{D}}z}\left[1-\operatorname{erf}\left(\frac{-z+\sqrt{s^2+4RDt}}{2\sqrt{Dt}}\right)\right]\right\} \tag{B.12}$$

Note that this expression satisfies the initial and boundary conditions when $t = 0$ and $z = 0$. It approaches the steady state profile as $t \to \infty$.

REFERENCES

Adams J. E. and Rhodes M. L. (1960) Dolomitization by seepage refluxion. *AAPG Bull.* **44**(12), 1912–1920.

Aulstead K. L., Spencer R. J. and Krouse H. R. (1988) Fluid inclusion and isotopic evidence on dolomitization, Devonian of Western Canada. *Geochim. Cosmochim. Acta* **52**(5), 1027–1035.

Azmy K., Lavoie D., Wang Z., Brand U., Al-Aasm I., Jackson S. and Girard I. (2013) Magnesium-isotope and REE compositions of Lower Ordovician carbonates from eastern Laurentia: implications for the origin of dolomites and limestones. *Chem. Geol.* **356**, 64–75.

Bartley J. K. and Kah L. C. (2004) Marine carbon reservoir, Corg-Ccarb coupling, and the evolution of the Proterozoic carbon cycle. *Geology* **32**(2), 129–132.

Boss S. K. and Wilkinson B. H. (1991) Planktogenic/eustatic control on cratonic/oceanic carbonate accumulation. *J. Geol.* **99**(4), 497–513.

Boudreau B. P. (2011) *Diagenetic Models and Their Implementation: Modelling Transport and Reactions in Aquatic Sediments*. Springer London, Limited, Berlin, Heidelberg, New York, London, Paris, Tokyo, Hong Kong.

Budd D. A. (1997) Cenozoic dolomites of carbonate islands: their attributes and origin. *Earth Sci. Rev.* **42**(1–2), 1–47.

Buhl D., Immenhauser A., Smeulders G., Kabiri L. and Richter D. K. (2007) Time series δ^{26}Mg analysis in speleothem calcite: kinetic versus equilibrium fractionation, comparison with other proxies and implications for palaeoclimate research. *Chem. Geol.* **244**(3–4), 715–729.

Canfield D. E. (1998) A new model for Proterozoic ocean chemistry. *Nature* **396**(6710), 450–453.

Carpenter J. H. and Manella M. E. (1973) Magnesium to chlorinity ratios in seawater. *J. Geophys. Res.* **78**(18), 3621–3626.

Chu X., Zhang T., Zhang Q. and Lyons T. W. (2007) Sulfur and carbon isotope records from 1700 to 800 Ma carbonates of the Jixian section, northern China: implications for secular isotope variations in Proterozoic seawater and relationships to global supercontinental events. *Geochim. Cosmochim. Acta* **71**(19), 4668–4692.

Fantle M. S. and DePaolo D. J. (2007) Ca isotopes in carbonate sediment and pore fluid from ODP Site 807A: the Ca^{2+}(aq)–calcite equilibrium fractionation factor and calcite recrystallization rates in Pleistocene sediments. *Geochim. Cosmochim. Acta* **71**(10), 2524–2546.

Fantle M. S. and Higgins J. (2014) The effects of diagenesis and dolomitization on Ca and Mg isotopes in marine platform carbonates: implications for the geochemical cycles of Ca and Mg. *Geochim. Cosmochim. Acta* **142**, 458–481.

Finch A. A. and Allison N. (2007) Coordination of Sr and Mg in calcite and aragonite. *Mineral. Mag.* **71**(5), 539–552.

Foster G. L., Pogge von Strandmann P. A. E. and Rae J. W. B. (2010) Boron and magnesium isotopic composition of seawater. *Geochem. Geophys. Geosyst.* **11**(8), Q08015. http://dx.doi.org/10.1029/2010gc003201.

Galy A., Bar-Matthews M., Halicz L. and O'Nions R. K. (2002) Mg isotopic composition of carbonate: insight from speleothem formation. *Earth Planet. Sci. Lett.* **201**(1), 105–115.

Galy A., Yoffe O., Janney P. E., Williams R. W., Cloquet C., Alard O., Halicz L., Wadhwa M., Hutcheon I. D., Ramon E. and Carignan J. (2003) Magnesium isotope heterogeneity of the isotopic standard SRM980 and new reference materials for magnesium-isotope-ratio measurements. *J. Anal. At. Spectrom.* **18**, 1352–1356.

Gao L.-Z., Ding X.-Z., Pang W.-H. and Zhang C.-H. (2010) New geologic time scale of Meo- and Neoproterozoic of China and geochronological constraint by SHRIMP zircon U–Pb dating. *J. Stratigr.* **35**(1), 1–7.

Geske A., Zorlu J., Richter D. K., Buhl D., Niedermayr A. and Immenhauser A. (2012) Impact of diagenesis and low grade metamorphosis on isotope (δ^{26}Mg, δ^{13}C, δ^{18}O and ^{87}Sr/^{86}Sr) and elemental (Ca, Mg, Mn, Fe and Sr) signatures of Triassic sabkha dolomites. *Chem. Geol.* **332–333**, 45–64.

Geske A., Goldstein R. H., Mavromatis V., Richter D. K., Buhl D., Kluge T., John C. M. and Immenhauser A. (2015a) The magnesium isotope (δ^{26}Mg) signature of dolomites. *Geochim. Cosmochim. Acta* **149**, 131–151.

Geske A., Lokier S., Dietzel M., Richter D. K., Buhl D. and Immenhauser A. (2015b) Magnesium isotope composition of sabkha pore water and related (Sub-) recent stoichiometric dolomites, Abu Dhabi (UAE). *Chem. Geol.* **393–394**, 112–124.

Given R. K. and Wilkinson B. H. (1987) Dolomite abundance and stratigraphic age: constraints on rates and mechanisms of Phanerozoic dolostone formation. *J. Sediment. Res.* **57**(6), 1068–1078.

Grotzinger J. P. and Kasting J. F. (1993) New constraints on Precambrian ocean composition. *J. Geol.* **101**(2), 235–243.

Grotzinger J. P. and Knoll A. H. (1995) Anomalous carbonate precipitates: is the Precambrian the key to the Permian?. *Palaios* **10**(6) 578–596.

Grotzinger J. P. and Knoll A. H. (1999) Stromatolites in Precambrian carbonates: evolutionary mileposts or environmental dipsticks? *Annu. Rev. Earth Planet. Sci.* **27**(1), 313–358.

Grotzinger J. P., Watters W. A. and Knoll A. H. (2000) Calcified metazoans in thrombolite–stromatolite reefs of the terminal Proterozoic Nama Group, Namibia. *Paleobiology* **26**(3), 334–359.

Hanshaw B. B., Back W. and Deike R. G. (1971) A geochemical hypothesis for dolomitization by ground water. *Econ. Geol.* **66**(5), 710–724.

Hardie L. A. (1996) Secular variation in seawater chemistry: an explanation for the coupled secular variation in the mineralogies of marine limestones and potash evaporites over the past 600 m.y. *Geology* **24**(3), 279–283.

Higgins J. A. and Schrag D. P. (2010) Constraining magnesium cycling in marine sediments using magnesium isotopes. *Geochim. Cosmochim. Acta* **74**(17), 5039–5053.

Higgins J. A. and Schrag D. P. (2012) Records of Neogene seawater chemistry and diagenesis in deep-sea carbonate sediments and pore fluids. *Earth Planet. Sci. Lett.* **357–358**, 386–396.

Higgins J. A. and Schrag D. P. (2015) The Mg isotopic composition of Cenozoic seawater – evidence for a link between Mg-clays, seawater Mg/Ca, and climate. *Earth Planet. Sci. Lett.* **416**, 73–81.

Hippler D., Buhl D., Witbaard R., Richter D. K. and Immenhauser A. (2009) Towards a better understanding of magnesium-isotope ratios from marine skeletal carbonates. *Geochim. Cosmochim. Acta* **73**(20), 34–6146.

Hoefs J. (2009) *Stable Isotope Geochemistry*, Sixth ed. Springer Verlag, Berlin, Heidelberg.

Holland H. D. and Zimmermann H. (2000) The dolomite problem revisited. *Int. Geol. Rev.* **42**(6), 481–490.

Holland H. D., Lazar B. and McCaffrey M. (1986) Evolution of the atmosphere and oceans. *Nature* **320**(6057), 27–33.

Hood A. v. S., Wallace M. W. and Drysdale R. N. (2011) Neoproterozoic aragonite–dolomite seas? Widespread marine dolomite precipitation in Cryogenian reef complexes. *Geology* **39**(9), 871–874.

Huang F., Zhang Z., Lundstrom C. C. and Zhi X. (2011) Iron and magnesium isotopic compositions of peridotite xenoliths from Eastern China. *Geochim. Cosmochim. Acta* **75**, 3318–3334.

Immenhauser A., Buhl D., Richter D., Niedermayr A., Riechelmann D., Dietzel M. and Schulte U. (2010) Magnesium-isotope fractionation during low-Mg calcite precipitation in a limestone cave – field study and experiments. *Geochim. Cosmochim. Acta* **74**(15), 4346–4364.

Jacobson A. D., Zhang Z., Lundstrom C. and Huang F. (2010) Behavior of Mg isotopes during dedolomitization in the Madison Aquifer, South Dakota. *Earth Planet. Sci. Lett.* **297**(3–4), 446–452.

Kah L. C. and Riding R. (2007) Mesoproterozoic carbon dioxide levels inferred from calcified cyanobacteria. *Geology* **35**(9), 799–802.

Kasemann S. A., Pogge von Strandmann P. A. E., Prave A. R., Fallick A. E., Elliott T. and Hoffmann K.-H. (2014) Continental weathering following a Cryogenian glaciation: evidence from calcium and magnesium isotopes. *Earth Planet. Sci. Lett.* **396**, 66–77.

Kaufman A. J. and Knoll A. H. (1995) Neoproterozoic variations in the C-isotope composition of sea water: stratigraphic and biogeochemical implications. *Precambr. Res.* **73**(3–4), 27–49.

Kaufman A. J. and Xiao S. (2003) High CO_2 levels in the Proterozoic atmosphere estimated from analyses of individual microfossils. *Nature* **425**(6955), 279–282.

Kaufman A. J., Corsetti F. A. and Varni M. A. (2007) The effect of rising atmospheric oxygen on carbon and sulfur isotope anomalies in the Neoproterozoic Johnnie Formation, Death Valley, USA. *Chem. Geol.* **237**(1–2), 47–63.

Land L. (1992) The dolomite problem: stable and radiogenic isotope clues. In *Isotopic Signatures and Sedimentary Records* (eds. N. Clauer and S. Chaudhuri). Springer, Berlin, Heidelberg, pp. 49–68.

Land L. (1998) Failure to precipitate dolomite at 25 °C from dilute solution despite 1000-fold oversaturation after 32 years. *Aquat. Geochem.* **4**(3–4), 361–368.

Last W. M. (1990) Lacustrine dolomite—an overview of modern, Holocene, and Pleistocene occurrences. *Earth Sci. Rev.* **27**(3), 221–263.

Lavoie D., Jackson S. and Girard I. (2014) Magnesium isotopes in high-temperature saddle dolomite cements in the lower Paleozoic of Canada. *Sediment. Geol.* **305**, 58–68.

Li Y.-H. and Gregory S. (1974) Diffusion of ions in sea water and in deep-sea sediments. *Geochim. Cosmochim. Acta* **38**(5), 703–714.

Li W., Chakraborty S., Beard B. L., Romanek C. S. and Johnson C. M. (2012) Magnesium isotope fractionation during precipitation of inorganic calcite under laboratory conditions. *Earth Planet. Sci. Lett.* **333–334**, 304–316.

Li W., Beard B. L., Li C. and Johnson C. M. (2014) Magnesium isotope fractionation between brucite [Mg(OH)2] and Mg aqueous species: implications for silicate weathering and biogeochemical processes. *Earth Planet. Sci. Lett.* **394**, 82–93.

Li W., Beard B. L., Li C., Xu H. and Johnson C. M. (2015) Experimental calibration of Mg isotope fractionation between dolomite and aqueous solution and its geological implications. *Geochim. Cosmochim. Acta* **157**, 164–181.

Ling M.-X., Sedaghatpour F., Teng F.-Z., Hays P. D., Strauss J. and Sun W. (2011) Homogeneous magnesium isotopic composition of seawater: an excellent geostandard for Mg isotope analysis. *Rapid Commun. Mass Spectrom.* **25**(19), 2828–2836.

Liu C., Wang Z., Raub T. D., Macdonald F. A. and Evans D. A. D. (2014) Neoproterozoic cap-dolostone deposition in stratified glacial meltwater plume. *Earth Planet. Sci. Lett.* **404**, 22–32.

Lu S., Zhao G., Wang H. and Hao G. (2008) Precambrian metamorphic basement and sedimentary cover of the North China Craton: a review. *Precambrian Res.* **160**(1–2), 77–93.

Lyons T. W., Reinhard C. T. and Planavsky N. J. (2014) The rise of oxygen in Earth/'s early ocean and atmosphere. *Nature* **506**(7488), 307–315.

Machel H. G. (2004) Concepts and models of dolomitization: a critical reappraisal. *Geol. Soc. Lond. Spec. Publ.* **235**(1), 7–63.

Mackenzie F. T. and Morse J. W. (1992) Sedimentary carbonates through Phanerozoic time. *Geochim. Cosmochim. Acta* **56**(8), 3281–3295.

Mathieu J., Kontak D. J. and Turner E. C. (2013) A fluid inclusion study of diagenetic fluids in Proterozoic and Paleozoic carbonate rocks, Victoria Island, NWT. *Geofluids* **13**(4), 559–578.

Mavromatis V., Gautier Q., Bosc O. and Schott J. (2013) Kinetics of Mg partition and Mg stable isotope fractionation during its incorporation in calcite. *Geochim. Cosmochim. Acta* **114**, 188–203.

Mavromatis V., Meister P. and Oelkers E. H. (2014) Using stable Mg isotopes to distinguish dolomite formation mechanisms: a case study from the Peru Margin. *Chem. Geol.* **385**, 84–91.

Mazzullo S. J. (2000) Organogenic dolomitization in peritidal to deep-sea sediments. *J. Sediment. Res.* **70**(1), 10–23.

McKenzie J. A. and Vasconcelos C. (2009) Dolomite Mountains and the origin of the dolomite rock of which they mainly consist: historical developments and new perspectives. *Sedimentology* **56**(1), 205–219.

Mei M., Ma Y., Guo Q. and Fei Z. (2001) Basic lithofacies-succession model for the Wumishan cyclothems: their markov chain analysis and regularly vertical stacking patterns in the third-order sequences. *Acta Geol. Sin. Engl. Ed.* **75**(4), 421–431.

Mei M., Gao J., Meng Q. and Liu Z. (2010) Sedimentary features and their implications of microdigital stromatolites from the mesoproterozoic Wumishan Formation at the Jixian section in North China. *Acta Geol. Sin. Engl. Ed.* **84**(3), 483–496.

Morris S. C., Mattes B. W. and Menge C. (1990) The early skeletal organism Cloudina: new occurrences from Oman and possibly China. *Am. J. Sci.* **290-A**, 245–260.

Mucci A. and Morse J. W. (1983) The incorporation of Mg^{2+} and Sr^{2+} into calcite overgrowths: influences of growth rate and solution composition. *Geochim. Cosmochim. Acta* **47**(2), 217–233.

Müller M. N., Kısakürek B., Buhl D., Gutperlet R., Kolevica A., Riebesell U., Stoll H. and Eisenhauer A. (2011) Response of the coccolithophores *Emiliania huxleyi* and *Coccolithus braarudii* to changing seawater Mg^{2+} and Ca^{2+} concentrations: Mg/Ca, Sr/Ca ratios and $\delta^{44/40}Ca$, $\delta^{26/24}Mg$ of coccolith calcite. *Geochim. Cosmochim. Acta* **75**(8), 2088–2102.

Pearce C. R., Saldi G. D., Schott J. and Oelkers E. H. (2012) Isotopic fractionation during congruent dissolution, precipitation and at equilibrium: evidence from Mg isotopes. *Geochim. Cosmochim. Acta* **92**, 170–183.

Planchon F., Poulain C., Langlet D., Paulet Y.-M. and André L. (2013) Mg-isotopic fractionation in the manila clam (*Ruditapes philippinarum*): new insights into Mg incorporation pathway and calcification process of bivalves. *Geochim. Cosmochim. Acta* **121**, 374–397.

Plummer L. N., Busenberg E., Drenkard S., Schlosser P., Ekwurzel B., Weppernig R., McConnell J. B. and Michel R. L. (1998) Flow of river water into a karstic limestone aquifer-2. Dating the young fraction in groundwater mixtures in the Upper Floridan aquifer near Valdosta, Georgia. *Appl. Geochem.* **13**(8), 1017–1043.

Pogge von Strandmann P. A. E. (2008) Precise magnesium isotope measurements in core top planktic and benthic foraminifera. *Geochem. Geophys. Geosyst.* **9**(12), Q12015. http://dx.doi.org/10.1029/2008gc002209.

Pogge von Strandmann P. A. E., Forshaw J. and Schmidt D. N. (2014) Modern and cenozoic records of magnesium behaviour from foraminiferal Mg isotopes. *Biogeosci. Discuss.* **11**(5), 7451–7484.

Pokrovsky B. G., Mavromatis V. and Pokrovsky O. S. (2011) Co-variation of Mg and C isotopes in Late Precambrian carbonates of the Siberian Platform: a new tool for tracing the change in weathering regime? *Chem. Geol.* **290**(1–2), 67–74.

Ra K., Kitagawa H. and Shiraiwa Y. (2010) Mg isotopes and Mg/Ca values of coccoliths from cultured specimens of the species *Emiliania huxleyi* and *Gephyrocapsa oceanica*. *Mar. Micropaleontol.* **77**(3–4), 119–124.

Reinhard C. T., Planavsky N. J., Robbins L. J., Partin C. A., Gill B. C., Lalonde S. V., Bekker A., Konhauser K. O. and Lyons T. W. (2013) Proterozoic ocean redox and biogeochemical stasis. *Proc. Natl. Acad. Sci. U.S.A.* **110**(14), 5357–5362.

Ren G.-X., Meng X.-H., Ge M., Wang D.-H. and Guo F. (2007) Origin of siliceous rock in Wumishan Formation, Jixian, Tianjin. *Geol. Sci. Technol. Inf.* **26**(5), 11–16.

Richter F. M. and DePaolo D. J. (1987) Numerical models for diagenesis and the Neogene Sr isotopic evolution of seawater from DSDP Site 590B. *Earth Planet. Sci. Lett.* **83**(1–4), 27–38.

Richter F. M., Mendybaev R. A., Christensen J. N., Hutcheon I. D., Williams R. W., Sturchio N. C. and Beloso, Jr., A. D. (2006) Kinetic isotopic fractionation during diffusion of ionic species in water. *Geochim. Cosmochim. Acta* **70**(2), 277–289.

Riding R. (2000) Microbial carbonates: the geological record of calcified bacterial–algal mats and biofilms. *Sedimentology* **47**, 179–214.

Roberts J. A., Kenward P. A., Fowle D. A., Goldstein R. H., González L. A. and Moore D. S. (2013) Surface chemistry allows for abiotic precipitation of dolomite at low temperature. *Proc. Natl. Acad. Sci. U.S.A.* **110**(36), 14540–14545.

Rosen M. R., Miser D. E., Starcher M. A. and Warren J. K. (1989) Formation of dolomite in the Coorong region, South Australia. *Geochim. Cosmochim. Acta* **53**(3), 661–669.

Rustad J. R., Casey W. H., Yin Q.-Z., Bylaska E. J., Felmy A. R., Bogatko S. A., Jackson V. E. and Dixon D. A. (2010) Isotopic fractionation of Mg^{2+}(aq), Ca^{2+}(aq), and Fe^{2+}(aq) with carbonate minerals. *Geochim. Cosmochim. Acta* **74**(22), 6301–6323.

Saenger C. and Wang Z. (2014) Magnesium isotope fractionation in biogenic and abiogenic carbonates: implications for paleoenvironmental proxies. *Quat. Sci. Rev.* **90**, 1–21.

Saenger C., Wang Z., Gaetani G., Cohen A. and Lough J. M. (2013) The influence of temperature and vital effects on magnesium isotope variability in Porites and Astrangia corals. *Chem. Geol.* **360–361**, 105–117.

Saulnier S., Rollion-Bard C., Vigier N. and Chaussidon M. (2012) Mg isotope fractionation during calcite precipitation: an experimental study. *Geochim. Cosmochim. Acta* **91**, 75–91.

Schauble E. A. (2004) Applying stable isotope fractionation theory to new systems. *Rev. Mineral. Geochem.* **55**(1), 65–111.

Schauble E. A. (2011) First-principles estimates of equilibrium magnesium isotope fractionation in silicate, oxide, carbonate and hexaaquamagnesium(2+) crystals. *Geochim. Cosmochim. Acta* **75**(3), 844–869.

Scholle P. A., Bebout D. G. and Moore C. H. (1983) *Carbonate Depositional Environments*. American Association of Petroleum Geologists, Tulsa, Oklahoma, U.S.A.

Schulz H. D. and Zabel M. (2006) *Marine Geochemistry*. Springer, Germany.

Scoffin T. P. (1987) *An Introduction to Carbonate Sediments and Rocks*. Chapman and Hall, New York, USA.

Shen B., Jacobsen B., Lee C.-T. A., Yin Q.-Z. and Morton D. M. (2009) The Mg isotopic systematics of granitoids in continental arcs and implications for the role of chemical weathering in crust formation. *Proc. Natl. Acad. Sci. U.S.A.* **106**(49), 20652–20657.

Shen B., Wimpenny J., Lee C.-T. A., Tollstrup D. and Yin Q.-Z. (2013) Magnesium isotope systematics of endoskarns: implications for wallrock reaction in magma chambers. *Chem. Geol.* **356**, 209–214.

Sibley D. F. (1991) Secular changes in the amount and texture of dolomite. *Geology* **19**(2), 151–154.

Sibley D. F. and Gregg J. M. (1987) Classification of dolomite rock textures. *J. Sediment. Res.* **57**(6), 967–975.

Tang D., Shi X. and Jiang G. (2013) Mesoproterozoic biogenic thrombolites from the North China platform. *Int. J. Earth Sci.* **102**(2), 401–413.

Teng F. -Z., Li W. -Y., Ke S., Yang W., Liu S. -A., Sedaghatpour F., Wang S. -J., Huang K. -J., Hu Y., Ling M. -X., Xiao Y., Liu X. -M., Li X. -W., Gu H. -O., Sio C. K., Wallace D. A., Su B. -X., Zhao L., Chamberlin J., Harrington M., Brewer A. (2015) Magnesium isotopic compositions of international geostandards. *Geostand. Geoanal. Res.* (in press).

Tipper E. T., Galy A., Gaillardet J., Bickle M. J., Elderfield H. and Carder E. A. (2006) The magnesium isotope budget of the modern ocean: constraints from riverine magnesium isotope ratios. *Earth Planet. Sci. Lett.* **250**(1–2), 241–253.

Tucker M. E. (1982) Precambrian dolomites: petrographic and isotopic evidence that they differ from Phanerozoic dolomites. *Geology* **10**(1), 7–12.

Tucker M. E. (1983) Diagenesis, geochemistry, and origin of a Precambrian dolomite; the Beck Spring Dolomite of eastern California. *J. Sediment. Res.* **53**(4), 1097–1119.

Tucker M. E. and Wright V. P. (1990) *Carbonate Sedimentology*. Wiley-Blackwell, Oxford, UK.

Vasconcelos C. and McKenzie J. A. (1997) Microbial mediation of modern dolomite precipitation and diagenesis under anoxic conditions (Lagoa Vermelha, Rio de Janeiro, Brazil). *J. Sediment. Res.* **67**(3), 378–390.

Vasconcelos C., McKenzie J. A., Bernasconi S., Grujic D. and Tiens A. J. (1995) Microbial mediation as a possible mechanism for natural dolomite formation at low temperatures. *Nature* **377**(6546), 220–222.

Wang S.-J., Teng F.-Z., Williams H. M. and Li S.-G. (2012a) Magnesium isotopic variations in cratonic eclogites: origins and implications. *Earth Planet. Sci. Lett.* **359–360**, 219–226.

Wang Z., Hu P., Gaetani G., Liu C., Saenger C., Cohen A. and Hart S. (2012b) Experimental calibration of Mg isotope fractionation between aragonite and seawater. *Geochim. Cosmochim. Acta* **102**, 113–123.

Warren J. (2000) Dolomite: occurrence, evolution and economically important associations. *Earth-Sci. Rev.* **52**(1–3), 1–81.

Warthmann R., van Lith Y., Vasconcelos C. g., McKenzie J. A. and Karpoff A. M. (2000) Bacterially induced dolomite precipitation in anoxic culture experiments. *Geology* **28**(12), 1091–1094.

Whitaker F. F., Smart P. L. and Jones G. D. (2004) Dolomitization: from conceptual to numerical models. *Geol. Soc. Lond. Spec. Publ.* **235**(1), 99–139.

Wombacher F., Eisenhauer A., Böhm F., Gussone N., Regenberg M., Dullo W. C. and Rüggeberg A. (2011) Magnesium stable isotope fractionation in marine biogenic calcite and aragonite. *Geochim. Cosmochim. Acta* **75**(19), 5797–5818.

Xiao S., Knoll A. H., Kaufman A. J., Yin L. and Zhang Y. (1997) Neoproterozoic fossils in Mesoproterozoic rocks? Chemostratigraphic resolution of a biostratigraphic conundrum from the North China Platform. *Precambrian Res.* **84**(3–4), 197–220.

Yoshimura T., Tanimizu M., Inoue M., Suzuki A., Iwasaki N. and Kawahata H. (2011) Mg isotope fractionation in biogenic carbonates of deep-sea coral, benthic foraminifera, and hermatypic coral. *Anal. Bioanal. Chem.* **40**(9), 2755–2769.

Young E. D. and Galy A. (2004) The isotope geochemistry and cosmochemistry of magnesium. *Rev. Mineral. Geochem.* **55**, 197–230.

Zhang F., Xu H., Konishi H., Kemp J. M., Roden E. E. and Shen Z. (2012a) Dissolved sulfide-catalyzed precipitation of disordered dolomite: Implications for the formation mechanism of sedimentary dolomite. *Geochim. Cosmochim. Acta* **97**, 148–165.

Zhang F., Xu H., Konishi H., Shelobolina E. S. and Roden E. E. (2012b) Polysaccharide-catalyzed nucleation and growth of disordered dolomite: a potential precursor of sedimentary dolomite. *Am. Mineral.* **97**(4), 556–567.

Associate editor: Fang-zhen Teng